European Journal of
Mineralogy
Open Access

Compositional variation and zoning of epidote supergroup minerals in the Campi Flegrei geothermal field, Naples, Italy

Harvey E. Belkin[1] and Benedetto De Vivo[2,3]

[1]U.S. Geological Survey (Ret.), 12201 Sunrise Valley Dr., Reston, Virginia 20192, USA
[2]Pegaso Online University, Piazza Trieste e Trento 48, 80132 Naples, Italy
[3]Department of Geosciences, Virginia Tech, Blacksburg, Virginia 24061, USA

Correspondence: Harvey E. Belkin (harveybelkin@gmail.com)

Abstract. Authigenic epidote supergroups are an abundant accessory mineral in the calcium–aluminum silicate and thermometamorphic hydrothermal zones of the Campi Flegrei (Phlegraean Fields) geothermal field located west of Naples, Italy. Geothermal exploration for high-enthalpy fluid produced drill core and cuttings to ~ 3 km depth in the Mofete (MF1, MF2, MF5) and San Vito (SV1, SV3) wells, where measured downhole temperatures of epidote-bearing samples range from 270–350 °C and from 285–390 °C for the Mofete and San Vito areas, respectively. Two epidote group (epidote, clinozoisite), some rare earth element (REE)-bearing, and two allanite group (allanite-(Ce), ferriallanite-(Ce)) minerals were identified by electron microprobe. The allanite group is light rare earth element (LREE, La–Gd) enriched, Ce dominant, with REE + Y that varies from 30.59 wt %–14.32 wt %. Complex compositional variation such as oscillatory, sector, and complex (mixed) zoning is a ubiquitous feature observed in the epidote group, which occurs as veins, in vugs, as various size masses, and as isolated single crystals. Compositional zoning is caused by variable Fe $\leftrightarrow$ Al^{3+} substitution and X_{Fe} [(Fe^{3+}) / (Fe^{3+} + Al)] ranges from 0.06–0.33 (Fe^{3+} = 0.185–0.967 apfu). X_{Fe} tends to decrease with increasing temperature in the Mofete wells, but its distribution is more complex in the San Vito wells, which records recent fault displacement. The variety and complexity of the epidote supergroup zoning suggest rapid fluid composition and/or intensive parameter fluctuations in the local hydrothermal system.

1 Introduction

The Campi Flegrei area, located west of Naples, Italy, contains numerous hot springs, fumaroles, and other geothermal manifestations, which were well known before the Roman Empire (Giacomelli and Scandone, 2012). Geothermal exploration, in an attempt to locate a productive field similar to Larderello, was intermittently conducted from 1939 to 1954 but was unsuccessful. Carlino et al. (2012) present the history of geothermal exploration in the Neapolitan volcanic region. Extensive drilling and geophysical exploration programs were resumed in 1978 as a joint venture of the Italian national utilities AGIP and ENEL and the Italian Geodynamic Project (Rosi and Sbrana, 1987). Wells were drilled to a depth of ~ 3 km with concomitant coring, geophysics, and fluid sampling. Although significant geothermal electric power production was never achieved in the Campi Flegrei

region, this exploration stimulated widespread research (e.g., Guglielminetti, 1986; Guidi and Antonelli, 1989; De Vivo et al., 1989; Altaner et al., 1991; Zamora et al., 1994; Caprarelli et al., 1997).

As part of the research which evolved from this extensive drilling program, a detailed fluid inclusion study was carried out to better understand the evolution of the fluid composition and the thermal history of the geothermal field (De Vivo et al., 1989). We have used the results of this fluid inclusion study to better understand, in some wells, the variation in epidote group composition. As part of this study, core and chip samples from three Mofete (MF1, MF2, MF5) and two San Vito (SV1, SV3) wells (Fig. 1) were carefully examined for the occurrence of fluid inclusions and to determine their host mineralogy. Members of the epidote group, epidote and clinozoisite, were identified in many samples in the
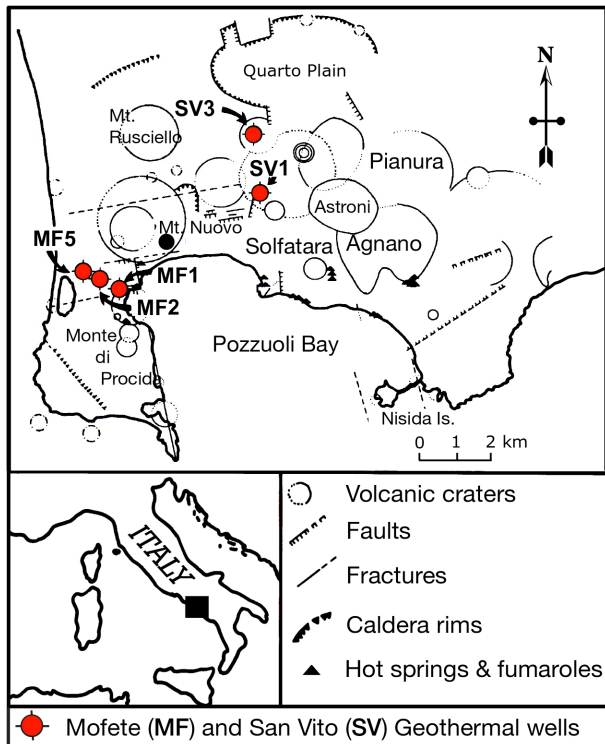
Figure 1. Schematic location map adapted from De Vivo et al. (1989) showing the Campi Flegrei caldera complex, various geologic features, and the positions of the five Mofete and San Vito geothermal wells (MF1, MF2, MF5, SV1, and SV3).

et al., 2020), a major event occurred in 39 ka (De Vivo et al., 2001) with the very large eruption ($\sim 310 \, \mathrm{km}^3$) of the Campanian Ignimbrite (Rolandi et al., 2003). Subsequent to this ignimbrite eruption, the Campi Flegrei region has had much volcanic activity ending with the Monte Nuovo eruption of 1538 CE (Rosi and Sbrana, 1987). For more detail regarding the volcanism of the Campi Flegrei area, the reader is referred to De Vivo et al. (2020) and Orsi et al. (2022) and chapters therein. Bradyseism and fumarolic activity continue, attesting to a still-active hydrothermal system (e.g., De Vivo and Lima, 2006; Bodnar et al., 2007; Lima et al., 2009; Bagnato et al., 2020; Lima et al., 2021; Chiodini et al., 2022). The chemistry of all the igneous products is Si-undersaturated, rich in alkalis, and low in MgO. Volumetrically, trachyte and alkali-trachyte are predominant with much lower amounts of trachybasalt, latite, and peralkaline–phonolitic–trachyte (Rosi and Sbrana, 1987). The chemistry of the rock penetrated by the Mofete and San Vito wells is generally similar from top to bottom although some wells (Fig. 2) end in hydrothermally metamorphosed marine marls, silts, and sandstones (Rosi and Sbrana, 1987). Piochi et al. (2014) give more stratigraphic detail on the MF5 and SV1 wells, and Mormone et al. (2011) provide more detail for the MF5 well.

3 Studied samples

All the samples came from the drilling program of AGIP and ENEL and include core and drill cuttings; however, the available samples were not a comprehensive selection of the core, especially for the shallower depths, but emphasized the deeper, hotter parts of the geothermal system. Thus, we do not have data for the shallower samples where epidote was identified by X-ray diffraction (XRD) and optical petrography (De Vivo et al., 1989). The Campi Flegrei geothermal system is liquid dominated with evidence of boiling and fluid reservoirs of different salinity (De Vivo et al., 1989; Caprarelli et al., 1997). The details of the studied samples are described in De Vivo et al. (1989). The studied samples containing epidote supergroups are listed in Table 1 and come from the Mofete 1 (MF1), Mofete 2 (MF2), Mofete 5 (MF5), San Vito 1 (SV1), and San Vito 3 (SV3) exploratory geothermal wells (Fig. 1). On the basis of detailed petrography and XRD determinations, Chelini and Sbrana (1987) defined four descending hydrothermal zones with different characteristic mineralogy: argillic, chlorite–illite, calcium–aluminum silicate, and the thermometamorphic zones. The calcium–aluminum silicate zone is characterized by abundant epidote, quartz, feldspars, various sulfides, and layered silicates. The top of this zone was stated by Chelini and Sbrana (1987) to be about 250 °C in the Mofete area and was less well defined in the San Vito area at between 220 and 270 °C (Fig. 2). The bottom of this zone was judged by Chelini and Sbrana (1987) to be at 325 °C in the Mofete area,

five studied wells and occurred throughout much of the core except at shallow depth. Preliminary studies (Belkin et al., 1990; Belkin and De Vivo, 2004) of their mineral chemistry revealed that their composition varied from epidote to clinozoisite and had different zoning textures. Two members of the allanite group, allanite-(Ce) and ferriallanite-(Ce), were also identified as authigenic phases in the core samples.

The specific aims of this report are (1) to document the composition and petrography of the epidote group in the Mofete and San Vito well samples, (2) to illustrate the various types of zoning observed in the epidote group, and (3) to document the composition and petrography of the allanite group. We know of no other compositional data for epidote supergroup minerals identified in the Mofete or San Vito geothermal fields.

2 Geologic setting of the Campi Flegrei region

The Campi Flegrei caldera complex (Fig. 1) is part of the active volcanic region developed on the subsiding western margin of the Apennine chain. This region also contains the Somma–Vesuvius, Procida, and Ischia volcanoes, not shown in Fig. 1. Although the region has been intermittently active during the last 600 kyr (Belkin et al., 2016; De Vivo
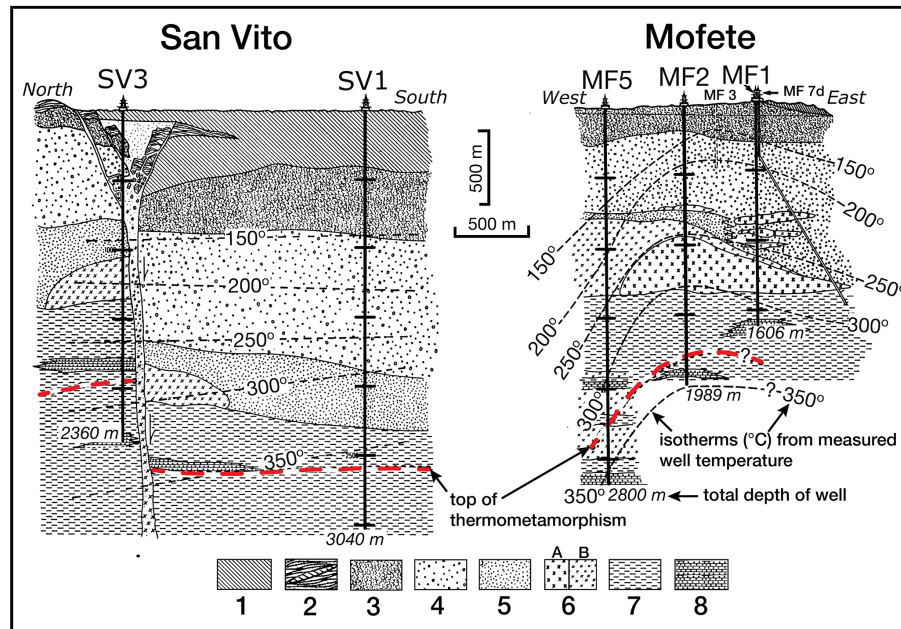
Figure 2. Schematic sketch showing generalized stratigraphy of the five geothermal wells, adapted from De Vivo et al. (1989). The top of thermometamorphism, total depth of well, and isotherms (°C) are indicated. Lithologic symbols: 1 – incoherent pyroclastic rocks; 2 – latitic soriae and pumices; 3 – yellow tuffs (post-caldera submarine activity); 4 – chaotic tuffites; 5 – chaotic tuffites (subaerial environment); 6A – trachytic lavas; 6B – latitic lavas and lava domes (pre-caldera period); 7 – interbedded tuffites, tuffs and lavas (submarine environment); and 8 – interbedded shales, marls, siltstones, and sandstones (marine).

whereas in San Vito 1 it corresponds to the current 360 °C isotherm, and in San Vito 3, it corresponds to the current 270 °C isotherm. This lower temperature in San Vito 3 reflects the complexity of recent faulting shifting older hydrothermal zones up and down (Fig. 2). The thermometamorphic zone is characterized by nearly complete recrystallization and/or replacement of the host rock; Chelini and Sbrana (1987) defined two subzones: amphibole–biotite and diopside. All the studied samples come from the calcium–aluminum silicate and the thermometamorphic zones as defined by Chelini and Sbrana (1987).

Recently, portions of the Mofete and San Vito cores have been examined in the following studies in order (1) to study the effects of water–rock reactions to aide in geochemical modeling (Piochi et al., 2021), (2) to develop a revised model for the subsurface structure of the Campi Flegrei (Piochi et al., 2014), and (3) to examine the secondary hydrothermal minerals in order to better understand the rock physics and state of the volcanic system (Mormone et al., 2011). Only in the studies by Mormone et al. (2011) and Piochi et al. (2021) is the epidote supergroup described as a component of the hydrothermal mineral assemblage, but no compositional data are given.

4 Nomenclature

In this report, we use the International Mineralogical Association (IMA)-recommended terminology as outlined by Armbruster et al. (2006) and Mills et al. (2009). The epidote supergroup is subdivided into groups, such as the epidote, allanite, and dollaseite groups. In our study, we identified only two members of the epidote group (clinozoisite, epidote) and two members of the allanite group (allanite-(Ce), ferriallanite-(Ce)). In the recommended nomenclature, the occupancy and dominance of key cation sites determine the group, root name, and individual species (Armbruster et al., 2006).

The epidote supergroup name assignment is based on the dominant valence at the M3, M1, and A2 sites and can be either M^{2+} or M^{3+}. The epidote group is defined as $[M^{2+}]_{A2} > 0.50$ and $[M^{3+}]_{M3} > 0.50$ (Armbruster et al., 2006). The distinction between clinozoisite and epidote is based on the dominance at the M3 site; $[Al^{3+}]_{M3} > 0.50$ is clinozoisite and $[Fe^{3+}]_{M3} > 0.50$ is epidote. For both clinozoisite and epidote, the dominant cations at the A1, A2, M1, and M2 sites are Ca, Ca, Al, and Al, respectively. We used the recommended metric $X_{Fe} = (Fe^{3+}) / (Fe^{3+} + Al)$ atoms per formula unit (apfu) to quantify the solid-solution members epidote and clinozoisite.

In the allanite group, A2 is occupied by $REE + Y + Th + U > A2^{2+}$ cations (REE denotes rare earth element) and the Levinson suffix indicates the dominant

Table 1. Distribution of epidote supergroup minerals in the Mofete and San Vito samples.

Sample	Depth (m)	Lithology	Alteration zone	T (°C)*	ep	czo	aln	faln
MF1-1150	1150	porphyritic trachyte	C	275	√		√	
MF1-1398	1398	porphyritic latite	C	305	√		√	
MF1-1495	1495	chaotic tuffite	C	320	√		√	
MF1-1597	1597	silty marl, sandstone	C	347	√	√	√	√
MF2-1582	1582	chaotic tuff	C	315	√		√	
MF2-1715	1715	chaotic tuff	C	325	√	√	√	
MF2-1824	1824	trachyte	C	335	√	√	√	
MF2-1960	1960	latite	D	345	√	√		
MF5-2605	2605	siltstone, sandstone	D	350	√	√		
SV1-2125	2125	chaotic tuff	C	300	√		√	
SV1-2510	2510	grey tuff	C	335	√		√	
SV1-2676	2676	grey tuff	D	350		√	√	
SV1-2860	2860	siltstone, sandstone	D	390	√			
SV3-2100	2100	chaotic tuffite	D	320	√			
SV3-2105	2105	chaotic tuffite	D	320	√	√		
SV3-2353	2353	siltstone, sandstone	D	330	√	√		
SV3-2359	2359	siltstone, sandstone	D	330	√	√		

ep, epidote; czo, clinozoisite; aln, allanite; faln, ferriallanite; C, calcium–aluminum silicate zone; D, thermometamorphic zone.
* Measured well temperature after stabilization (De Vivo et al., 1989).

rare earth element (REE + Y). In the IMA-recommended system (Armbruster et al., 2006), the allanite group is derived from the epidote group by homovalent substitutions and one coupled heterovalent substitution of the type $(REE)_{A2}^{3+} + M_{M3}^{2+} \rightarrow Ca_{A2}^{2+} + M_{M3}^{3+}$. Thus, the valences on the key sites, A2 and M3, are the reverse of the epidote group. Gieré and Sorensen (2004), in a comprehensive review of allanite and REE-bearing epidote mineralogy, point out that the distinction of allanite from REE-rich epidote differs by author. In the IMA procedure, REE-bearing epidote and clinozoisite are distinguished from allanite by the dominant cation(s) (> 0.50) in the A2 and M3 sites. The dominance of Fe^{3+} in the M1 site distinguishes ferriallanite from allanite.

To normalize the electron microprobe (electron probe microanalyzer, EPMA) data, we used the program WinEpclas (Yavuz and Yildirim, 2018), which follows the IMA-recommended naming procedure based on site occupancy and cation dominance. Normalization of EPMA data was on the basis of $\Sigma(T + M + A) = 8$ cations.

5   Analytical methods

Polished thin sections were prepared either from pieces of core or from individual hand-picked crystals. After routine optical petrography, the samples were examined with a JEOL JSM-840 scanning electron microscope (SEM) equipped with a Princeton Gamma-Tech Si(Li) energy-dispersive X-ray analyzer or a Hitachi SU5000 Schottky thermally as-

sisted field-emission SEM equipped with an Oxford Ultima 100 mm² energy-dispersive X-ray spectroscopy (EDS) silicon drift detector to select areas for analysis. Quantitative electron microprobe analyses of major and minor elements were obtained with a JEOL JXA-8900R five-spectrometer, fully automated EPMA using wavelength-dispersive X-ray spectrometry (WDS). Analyses were made at 15 keV accelerating voltage and 20 or 30 nA probe current measured with a Faraday cup, and counting times on both the peak and the background varied from 20 to 120 s.

Quantitative analyses of minerals containing rare earths are not trivial due to inherent peak overlap interferences, and various strategies to obtain good electron microprobe data have been described (e.g., Exley, 1980; Scherrer et al., 2000). A 15 keV accelerating voltage was used to reduce the potential of higher-order peak interference. Following the technique described by Exley (1980), $L\alpha$ for Y, La, Ce, Er, and Yb and $L\beta$ for Pr, Nd, Sm, Eu, Gd, and Dy were used with a LiF analyzing crystal. The analyses were corrected for electron beam matrix effects, instrumental drift, and dead time using a Phi-Rho-Z algorithm (CITZAF; Armstrong, 1995) as supplied with the JEOL JXA-8900R electron microprobe. Standards were appropriate synthetic or natural materials available in the Reston Electron Microbeam Laboratory (Huebner and Woodruff, 1985). The relative accuracy of the analyses, based upon comparison between measured and published compositions of standard reference materials, is ∼ 1 %–2 % for oxide concentration > 1 wt % and ∼ 5 %–10 % for oxide concentrations < 1 wt %. Elements analyzed

as oxides and their detection limits (wt %) at 3 standard deviations are as follows: MgO (0.02), Al_2O_3 (0.02), SiO_2 (0.02), CaO (0.02), TiO_2 (0.02), Cr_2O_3 (0.07), FeO (total) (0.03), PbO (0.09), Y_2O_3 (0.06), SrO (0.06), MnO (0.02), ThO_2 (0.09), Na_2O (0.02), K_2O (0.02), La_2O_3 (0.09), Ce_2O_3 (0.09), Nd_2O_3 (0.15), Pr_2O_3 (0.10), Sm_2O_3 (0.10), Eu_2O_3 (0.12), and Gd_2O_3 (0.10). Heavier REEs in REE-bearing epidote, allanite, or ferriallanite were not found above a detection limit of 0.15 wt %. Neither Cr_2O_3 nor PbO was detected in any analysis. The complete data sets for the epidote group and allanite group analyses are given in the Supplement.

6 Results – epidote group

Epidote and clinozoisite, members of the monoclinic epidote group, occur in a wide diversity of parageneses within a great range of pressures, temperatures, and host rock compositions (e.g., Zen and Hammarstrom, 1984; Deer et al., 1986; Bird and Spieler, 2004; Chen et al., 2019; Ahmed et al., 2020). The general formula for the epidote group minerals is $A_2M_3[T_2O_7][TO_4]O(OH)$ where the Fe^{3+} and Al endmembers are epidote $Ca_2(Al_2Fe^{3+})[Si_2O_7][SiO_4]O(OH)$ and clinozoisite $Ca_2Al_3[Si_2O_7][SiO_4]O(OH)$, respectively. Other cations can substitute in minor amounts; A sites can contain large, high-coordination cations such as Sr, Pb, REE, Y, Th, Na, and K, and octahedrally coordinated M sites can contain Mn^{3+}, Mn^{2+}, Fe^{2+}, Ti, Cr^{3+}, and V cations. REEs have been measured in the A2 site of epidote group minerals from a wide variety of paragenetic environments such as magmatic (Dawes, 1990), ultrahigh pressure (Rolfo et al., 2000), various metamorphic facies (Smulikowski and Kozłowski, 1994; see also Gieré and Sorensen, 2004), and geothermal (Aggarwal, 1999; Bird and Spieler, 2004).

6.1 Petrography

In the studied samples, the epidote group occurs in a wide variety of habits, shapes, and sizes. Very common throughout the cores were vugs (Fig. 3a) and veins containing hundreds to just a few crystals (Fig. 3b). Also, we observe crystal vugs completely or partially filled by later deposition of K-feldspar (Fig. 3c), quartz, and calcite. Limited optical petrographic study suggests that epidote crystals appear to be elongated in the *b*-crystallographic direction but have various aspect ratios. Some crystals were relatively stubby (Fig. 3c), and some had length-to-width ratios of as much as 10 : 1 (Fig. 3a). No systematic distribution of sizes as reported by Patrier et al. (1990) was found, but it appeared that the mode of occurrence influenced the size. Larger crystals are observed in larger veins or vugs, and smaller crystals are noted in the thinner veins and smaller pores. Another very common epidote group occurrence is in masses of crystals of up to 1.5 cm usually cored by another earlier phase (Fig. 4a, b). Sulfides, allanite-(Ce), ferriallanite-(Ce), cerite-

(Ce), aluminocerite-(Ce), titanite, britholite-(Ce), and a TiO_2 phase were observed in the cores of epidote group masses. Epidote was observed to fill probable vesicles with a well-defined outer edge (Fig. 4c) and partially filled cavities with a more irregular boundary (Fig. 4d). Veins, commonly transecting the thin section, were usually accompanied by pyrite or pyrrhotite (Fig. 4e), and the individual crystals comprising the veins were invariably zoned (Fig. 4f).

6.2 Epidote group composition

The clinozoisite (czo)–epidote (ep) members of the epidote group are related by the exchange of $Fe^{3+} \leftrightarrow Al$ in the M3 site; we used X_{Fe} [$Fe^{3+} / (Fe^{3+} + Al)$] apfu as a measure of this exchange.

6.2.1 Mofete samples

In the Mofete core samples, X_{Fe} ranged from 0.06 to 0.33, where MF1 varied from czo 0.15–0.16 to ep 0.18–0.33; MF2 varied from czo 0.11–0.16 to ep 0.17–0.27, and MF5 varied from czo 0.06–0.16 to ep 0.17–0.18 (X_{Fe}). The Mofete epidote group data show a good linear co-variation in the Fe^{3+}–Al substitution (Fig. 5a). Aluminum varies from 2.00–2.76 apfu, and Fe^{3+} varies from 0.967–0.185 apfu. Minor elements analyzed in Mofete clinozoisite and epidote were Ti, Mn, Mg, Sr, K, Na, Pb, Cr, Y, and Th. Manganese, Ti, Mg, and Sr were the most abundant, with MnO ranging (in wt %) from 0.04–2.00, TiO_2 ranging from the detection limit (dl)–0.34, MgO ranging from dl–0.37, and SrO ranging from dl–0.55. Potassium, Na, Y, and Th were very rarely detected, and Pb and Cr were not detected. Table 2 gives representative compositions of the Mofete epidote group.

6.2.2 San Vito samples

In the San Vito core samples, X_{Fe} ranged from 0.10 to 0.32, where SV1 varied for ep from 0.25–0.32 and for czo from 0.11–0.16 and SV3 ranged from czo 0.10–0.16 to ep 0.17–0.28 (X_{Fe}). The San Vito epidote group data show a good linear co-variation in the Fe^{3+}–Al substitution (Fig. 5b). Aluminum varies from 2.03–2.68 apfu, and Fe^{3+} varies from 0.939–0.295 apfu. Minor elements analyzed in San Vito clinozoisite and epidote were Ti, Mn, Mg, Sr, K, Na, Pb, Cr, Y, and Th. Manganese, Ti, Mg, and Sr were the most abundant, with MnO ranging (in wt %; dl denotes detection limit) from dl–0.85, TiO_2 ranging from dl–0.50, MgO ranging from dl–0.36, and SrO ranging from dl–0.48. Potassium, Na, and Y were very rarely detected with most analyses just above detection; Pb, Cr, Th, and Y were not detected. The minor elements in the San Vito epidote group were, in general, less abundant than in the Mofete epidote group. No major gap in X_{Fe} (Fig. 5a, b) that would suggest immiscibility (cf. Holdaway, 1972; Brunsmann et al., 2002) was observed in either the Mofete or the San Vito samples. Table 3 gives representative compositions of the San Vito epidote group.

Table 2. Representative compositions of epidote and clinozoisite from the Mofete samples.

Analysis	MFI-1150.49	MF2-1715xl.3	MF2-1824.14xl.B	MF2-1824.15xl.B	MF2-1824.13xl.B	MFI-1597xl.F	MFI-1597xl.B	MFI-1597xl.F	MF5-2605.3	MF5-2605.2	MF5-2605xl.A	MF5-2605xl.B
Depth (m)	1150	1715	1824	1824	1824	1597	1597	1597	2605	2605	2605	2605
Temperature (°C**)	275	325	335	335	335	347	347	347	350	350	350	350
Comment			low Z	intermediate Z	high Z edge	low Z		high Z				high Z
Figure and spot	core		Fig. 8b, G	Fig. 8b, H	Fig. 8b, I	Fig. 8d, J		Fig. 8d, K				
Mineral	ep	ep	czo	czo	ep	czo	czo	ep	czo	czo	ep	ep
n	1	3	1	1	3	2	3	3	1	1	2	1
SiO_2 (wt %)	37.50	38.45	39.30	39.18	38.49	38.52	39.19	37.54	39.16	38.98	38.40	38.85
TiO_2	bdl	0.11	0.16	0.05	0.05	bdl	0.08	bdl	0.09	0.02	0.03	0.07
Al_2O_3	21.30	24.69	28.50	27.99	24.97	27.45	27.40	24.59	30.38	29.86	27.03	26.45
FeO*	14.49	11.20	6.25	7.36	10.47	7.07	8.19	10.97	3.93	5.11	8.22	8.42
MgO	0.16	0.06	bdl	bdl	bdl	0.11	0.05	0.12	0.02	0.03	0.02	0.03
MnO	0.12	0.20	0.17	0.21	0.67	0.18	0.28	0.32	0.68	1.23	0.33	0.24
CaO	23.50	23.53	23.71	23.54	22.84	23.82	23.52	23.50	23.08	22.47	23.54	23.88
SrO	0.11	0.07	0.14	0.17	0.10	0.16	0.13	0.14	0.07	0.06	bdl	0.11
Total	97.18	98.31	98.23	98.50	97.59	97.30	98.84	97.18	97.41	97.76	97.57	98.05
Formulae on the basis of (T + M + A) = 8 cations												
Si	2.991	3.001	3.027	3.018	3.024	3.001	3.015	2.962	3.021	3.008	2.992	3.017
Ti	0.000	0.006	0.009	0.003	0.003	0.000	0.005	0.000	0.005	0.001	0.002	0.004
Al	2.002	2.271	2.587	2.541	2.312	2.520	2.485	2.286	2.762	2.716	2.482	2.421
Fe^{3+}	0.967	0.715	0.340	0.417	0.633	0.461	0.476	0.724	0.185	0.265	0.531	0.537
Fe^{2+}	0.000	0.016	0.062	0.057	0.055	0.000	0.051	0.000	0.069	0.065	0.004	0.010
Mg	0.019	0.007	0.000	0.000	0.000	0.013	0.006	0.014	0.002	0.003	0.002	0.003
Mn	0.008	0.013	0.011	0.014	0.045	0.012	0.018	0.021	0.044	0.080	0.022	0.016
Ca	2.008	1.968	1.957	1.943	1.923	1.988	1.939	1.986	1.908	1.858	1.965	1.987
Sr	0.005	0.003	0.006	0.008	0.005	0.007	0.006	0.006	0.003	0.003	0.000	0.005
X_{Fe}	0.33	0.24	0.12	0.14	0.21	0.15	0.16	0.24	0.06	0.09	0.18	0.18

* total iron as Fe^{2+}; bdl, below detection limit; Na_2O, K_2O, Y_2O_3, and ThO_2 are bdl; n, number of analyses averaged; $X_{Fe} = (Fe^{3+})/(Fe^{3+} + Al)$ apfu; ep, epidote; czo, clinozoisite. ** Temperatures from measured well temperatures (De Vivo et al., 1989). Fe^{3+}/Fe^{2+} is calculated on the basis of stoichiometry; Z, average atomic number.

Table 3. Representative compositions of epidote and clinozoisite from the San Vito samples.

Analysis	SV1-2125.6xl.B	SV3-2100.S	SV3-2105xl.1	SV3-2353Tr30	SV3-2353Tr47	SV3-2353Tr28	SV3-2353xl.Ar	SV3-2353xl.Ac	SV3-2353xl.Bc	SV1-2510.M	SV1-2676-11	SV1-2860xl.E
Depth m	2125	2100	2105	2353	2353	2353	2353	2353	2353	2510	2676	2860
Temperature (°C**)	300	320	320	330	330	330	330	330	330	335	350	390
Comment		small xl in vug					low Z rim	high Z core	high Z core	xl mass		
Figure and spot			Fig. 7c, D	Fig. 7a, F	Fig. 7c, E	Fig. 7b, B	Fig. 7b, C	Fig. 7a, A				
n	3	1	3	1	1	1	3	3	2	4	1	3
Mineral	ep	ep	ep	ep	czo	czo	czo	ep	ep	ep	czo	ep
SiO_2 (wt %)	37.46	37.73	38.53	38.80	39.40	39.23	38.81	38.13	38.02	37.35	37.71	38.56
TiO_2	0.73	0.05	0.03	0.07	0.17	0.06	bdl	bdl	0.03	0.14	0.16	0.16
Al_2O_3	21.58	24.79	26.15	25.40	29.53	27.99	27.72	24.09	23.73	23.92	27.43	23.36
FeO^*	13.79	11.21	9.59	10.43	5.46	7.43	7.35	11.73	12.21	12.77	5.59	12.68
MgO	0.02	0.31	0.07	0.17	0.02	0.14	0.16	0.03	0.06	0.29	bdl	bdl
MnO	0.38	0.06	0.11	0.21	0.02	0.12	0.08	0.06	0.05	0.85	0.49	0.32
CaO	22.57	22.96	23.48	23.51	24.01	23.61	23.72	23.33	23.23	21.88	22.24	23.26
SrO	0.14	bdl	0.16	bdl	bdl	bdl	0.15	bdl	0.08	bdl	0.48	0.07
Na_2O	bdl	bdl	0.02	bdl	bdl	bdl	bdl	0.02	bdl	bdl	0.07	bdl
Y_2O_3	bdl	bdl	bdl	bdl	bdl	bdl	bdl	bdl	bdl	bdl	0.39	bdl
Total	96.74	97.11	98.14	98.59	98.61	98.58	98.00	97.39	97.39	97.20	94.56	98.41
Formulae on the basis of $(T + M + A) = 8$ cations												
Si	3.008	2.975	2.996	3.010	3.011	3.015	3.001	3.007	3.003	2.961	3.026	3.023
Ti	0.044	0.003	0.002	0.004	0.010	0.003	0.001	0.001	0.002	0.008	0.010	0.009
Al	2.043	2.303	2.397	2.322	2.660	2.535	2.527	2.239	2.209	2.235	2.594	2.158
Fe^{3+}	0.851	0.739	0.611	0.650	0.298	0.427	0.462	0.748	0.781	0.827	0.329	0.777
Fe^{2+}	0.076	0.000	0.013	0.026	0.051	0.051	0.014	0.026	0.025	0.019	0.046	0.054
Mg	0.002	0.036	0.008	0.020	0.002	0.016	0.018	0.004	0.006	0.034	0.000	0.000
Mn	0.026	0.004	0.007	0.014	0.001	0.008	0.005	0.004	0.003	0.057	0.033	0.021
Ca	1.942	1.939	1.956	1.954	1.966	1.944	1.966	1.971	1.966	1.858	1.912	1.954
Sr	0.007	0.000	0.007	0.000	0.000	0.000	0.007	0.000	0.003	0.000	0.022	0.003
Na	0.000	0.000	0.003	0.000	0.000	0.000	0.000	0.002	0.000	0.000	0.011	0.000
Y	0.000	0.000	0.000	0.000	0.000	0.000	0.000	0.000	0.000	0.000	0.017	0.000
X_{Fe}	0.29	0.24	0.20	0.22	0.10	0.14	0.15	0.25	0.26	0.27	0.11	0.26

* Total iron as Fe^{2+}; bdl, below detection limit; K_2O and ThO_2 are bdl; n, number of analyses averaged; $X_{Fe} = (Fe^{3+})/(Fe^{3+} + Al)$ apfu; ep, epidote; czo, clinozoisite. ** Temperatures from measured well temperatures (De Vivo et al., 1989), Fe^{3+} / Fe^{2+} is calculated on the basis of stoichiometry; Z, average atomic number.
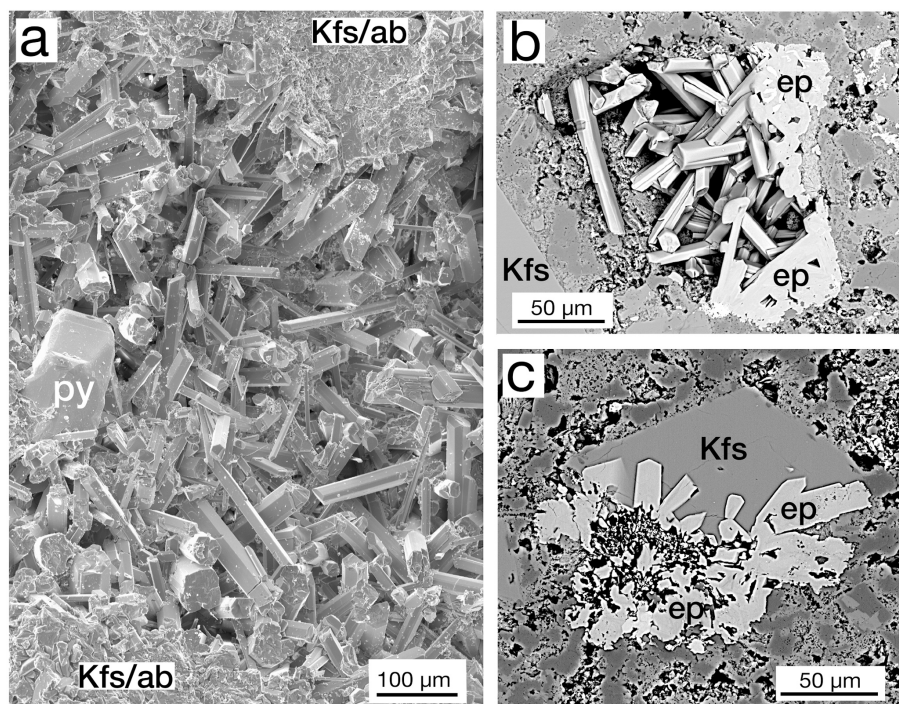
Figure 3. (a) Centimeter-size vug of epidote crystals in sample MF1-1597 in potassium feldspar and albite (Kfs/ab) with crystals of pyrite (py), SE image. **(b)** Vug in sample SV1-2125 containing crystals of epidote (ep) surrounded by K-feldspar (Kfs), backscattered electron (BSE) image. **(c)** Vug filled with epidote (ep) crystals subsequently filled by K-feldspar (Kfs), sample MF1-1495, BSE image.

6.3 Composition variation with temperature

Although we were limited by the number of Mofete and San Vito core samples, we observe a general decrease in X_{Fe} with increasing temperature and depth but only in the Mofete wells. In the Mofete wells, Fig. 6a shows that with increasing well temperature, X_{Fe} tends to decrease (i.e., more abundant clinozoisite) especially in the MF1 samples. In this well, we have a greater temperature and depth range of samples. The composition ranges in MF1 from epidote at 0.33 X_{Fe} at 275 °C (1150 m depth) to clinozoisite at 0.15 X_{Fe} at 347 °C (1597 m depth). The situation is much less clear in the San Vito wells (Fig. 6b), where there has been recent fault movement. In the SV1 well, all the epidote group minerals are epidote except at depth 2676 m, 350 °C. Except for this clinozoisite, the epidote composition does not change with temperature or depth given the limited available sampling. Sampling in the San Vito SV3 well varied from 2100–2359 m with a narrow range of well temperatures (320–333 °C). The wide spread of analyzed compositions at 330 °C (2353 m) resulted from the abundance of oscillatory zoned crystals observed in a vug and one that was analyzed along a traverse (see below).

6.4 Compositional zoning in the epidote group

Various styles of zoning in epidote group minerals were observed in all the studied Mofete and San Vito well samples. Zoning involving a smooth gradation either from a Fe-rich core to an Al-rich rim or vice versa was not observed. All the compositional zones were separated by relatively sharp boundaries, at least within the resolution limits of the SEM, although in some complex zoning areas, these were difficult to clearly resolve. We observed oscillatory, complex, and sector zoning.

Oscillatory zoning was most clearly observed when the crystal happened to lie lengthwise in the plane of the thin section. Figure 7a shows a portion of an 850 μm crystal oriented so that the oscillatory zoning is clearly displayed. The core (right arrow) is a partially resorbed epidote (spot A). In the same vug, Fig. 7b shows another partially resorbed core in a crystal oriented perpendicular to Fig. 7b. The core of Fig. 7b is iron-rich (spot C), but the crystal growth following the resorption was relatively iron-poor (spot B). Two traverses are conducted on the crystal in Fig. 7a: (1) WDS line scan recording the Fe $K\alpha$ and Al $K\alpha$ counts per second and (2) WDS analytical analysis every ~ 25 μm. Figure 7c shows the line scan across the variable-width oscillatory zones. Two zones, spots D (ep) and E (czo), are separated by a very sharp boundary, although because the microprobe beam has finite volume, the line scan transitions are somewhat sloped. Inset
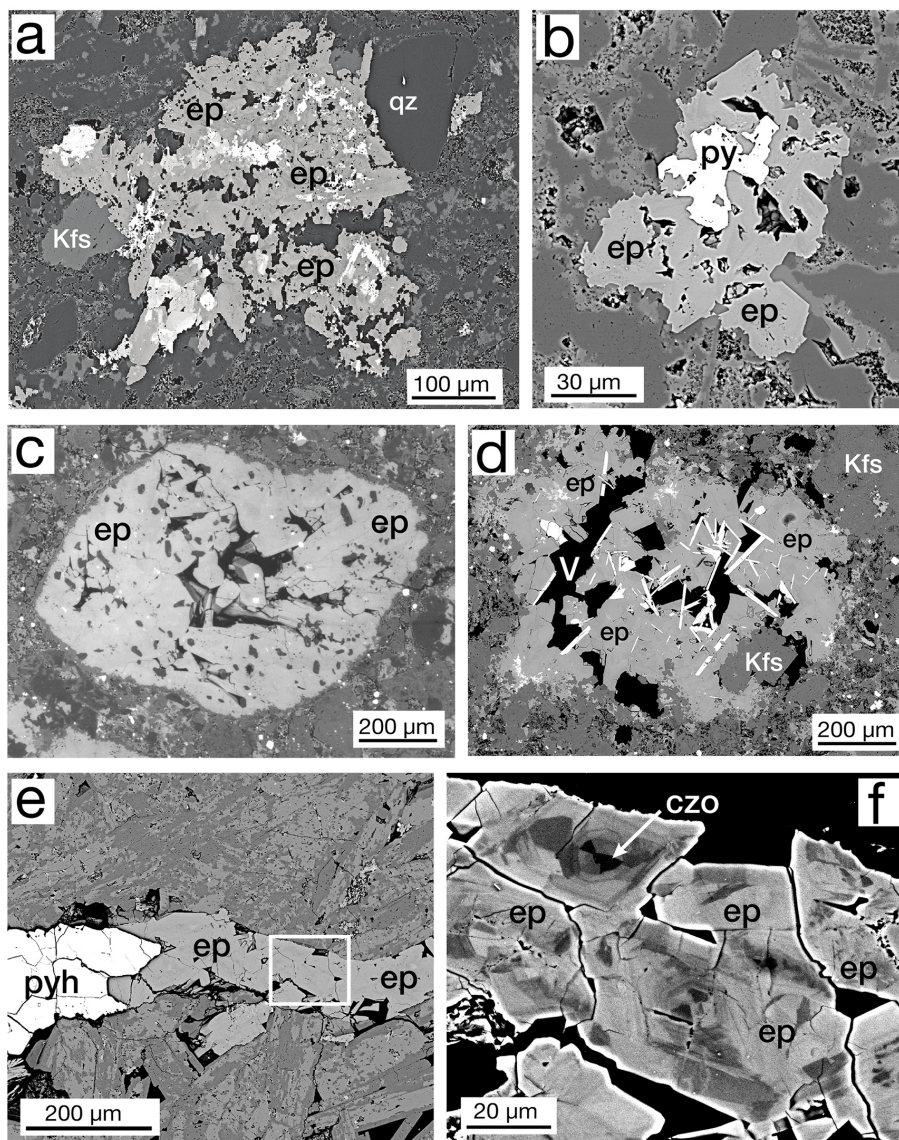
Figure 4. BSE images: **(a)** typical irregularly shaped mass of epidote (ep) crystals with quartz (qz) and K-feldspar (Kfs) from sample MF1-1597. Details of the bright core area are shown in Fig. 9f. **(b)** Mass of epidote crystals (ep) with pyrite (py), sample MF1-1495. **(c)** Probable vesicle filled with epidote (ep), sample SV1-2510. **(d)** Open cavity partially filled (V – vug) with epidote (ep) and potassium feldspar (Kfs) with hematite blades (high BSE), sample SV1-2510. **(e)** Portion of a > 2 cm pyrrhotite (pyh), clinozoisite, and epidote vein. Box enlarged in **(f)**, sample MF2-1824. **(f)** Enlarged area imaged with high BSE contrast to show complex patchy zoning of epidote (ep) and clinozoisite (czo).

Fig. 7d gives the X_{Fe} values measured by an EPMA at selected points; Table 3 gives their complete analysis.

Complex zoning was the most common type observed in both Mofete and San Vito samples and was usually mixed with other zoning types. It was recognized in crystals growing in vugs (Fig. 8a), in masses of crystals, and in veins (Fig. 4f). Figure 8a shows a portion of a vug (MF2-1824) with some of the crystals with britholite-(Ce) centers. The enlarged portion (Fig. 8b) of a euhedral crystal shows a chaotic assemblage of zones in the center that are terminated by os-cillatory zoning. Spots analyzed in Fig. 8b show that the center is iron-poor relative to the peripheral zones. Figure 8e gives the X_{Fe} data for selected spots, and their EPMA data are given in Table 2.

Sector zoning refers to a compositional difference between coeval growth sectors in a crystal. This type was less common than either complex or oscillatory zoning in the samples and was typically seen in crystals in vugs (Fig. 8c). Where measured by the EPMA, the different sectors had significantly different X_{Fe} values and BSE responses. The zoning
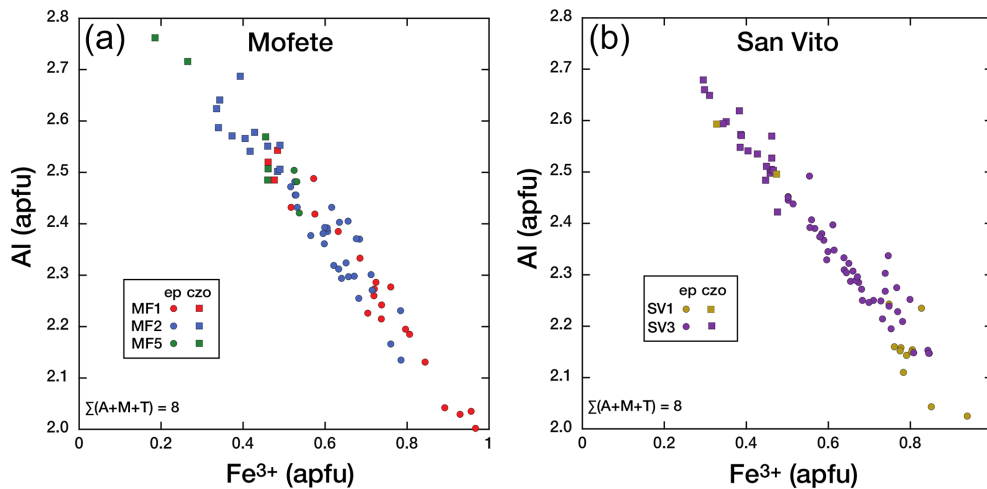
Figure 5. Co-variation in Al and Fe^{3+} (apfu) in the epidote group for the three Mofete cores (**a**) and the two San Vito cores (**b**). Epidote (ep) is shown as a solid circle and clinozoisite (czo) as a solid square.
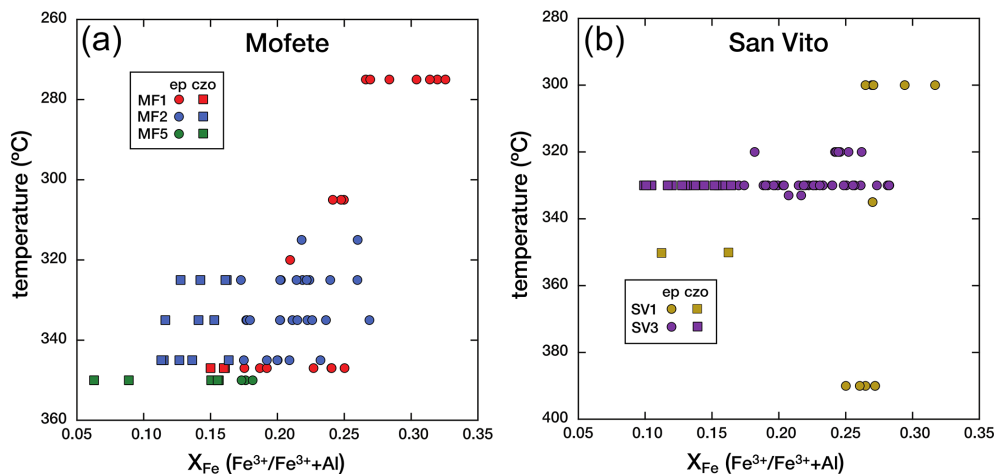

Figure 6. The variation in X_{Fe} $[(Fe^{3+}) / (Fe^{3+} + Al)]$ apfu in the epidote group with measured well-hole temperature (°C) after stabilization (De Vivo et al., 1989) for Mofete (**a**) and San Vito (**b**) wells. Symbols are as in Fig. 5a and b.

shown in Fig. 8d also illustrates the mixtures of zoning types: oscillatory and complex zoning with sector zoning in some of the late-formed crystals. The X_{Fe} values are shown in Fig. 8e and the complete EPMA data in Table 2.

Sector zoning refers to a compositional difference between coeval growth sectors in a crystal. This type was less common than either complex or oscillatory zoning in the samples and was typically seen in crystals in vugs (Fig. 8c). Where measured by the EPMA, the different sectors had significantly different X_{Fe} values and BSE responses. The zoning shown in Fig. 8d also illustrates the mixtures of zoning types: oscillatory and complex zoning with sector zoning in some of the late-formed crystals. The X_{Fe} values are shown in Fig. 8e and the complete EPMA data in Table 2.

7   Results – REE-bearing epidote supergroup

We have separated, for description, members of the allanite group from those of the epidote group that had detectable REE + Y. The critical distinction that separates the allanite group from other members of the epidote supergroup containing REE + Y is the dominance (> 50 % apfu) of REE + Y in the A2 site (Armbruster et al., 2006).

7.1   Allanite group

We identified two members of the allanite group, allanite-(Ce) $[CaCeAl_2Fe^{2+}[Si_2O_7] [SiO_4]O(OH)]$ and ferriallanite-(Ce) $[CaCeFe^{3+}AlFe^{2+}[Si_2O_7][SiO_4]O(OH)]$. Table 1 gives the distribution of the allanite group in the studied samples. The allanite group was much more abundant in the Mofete
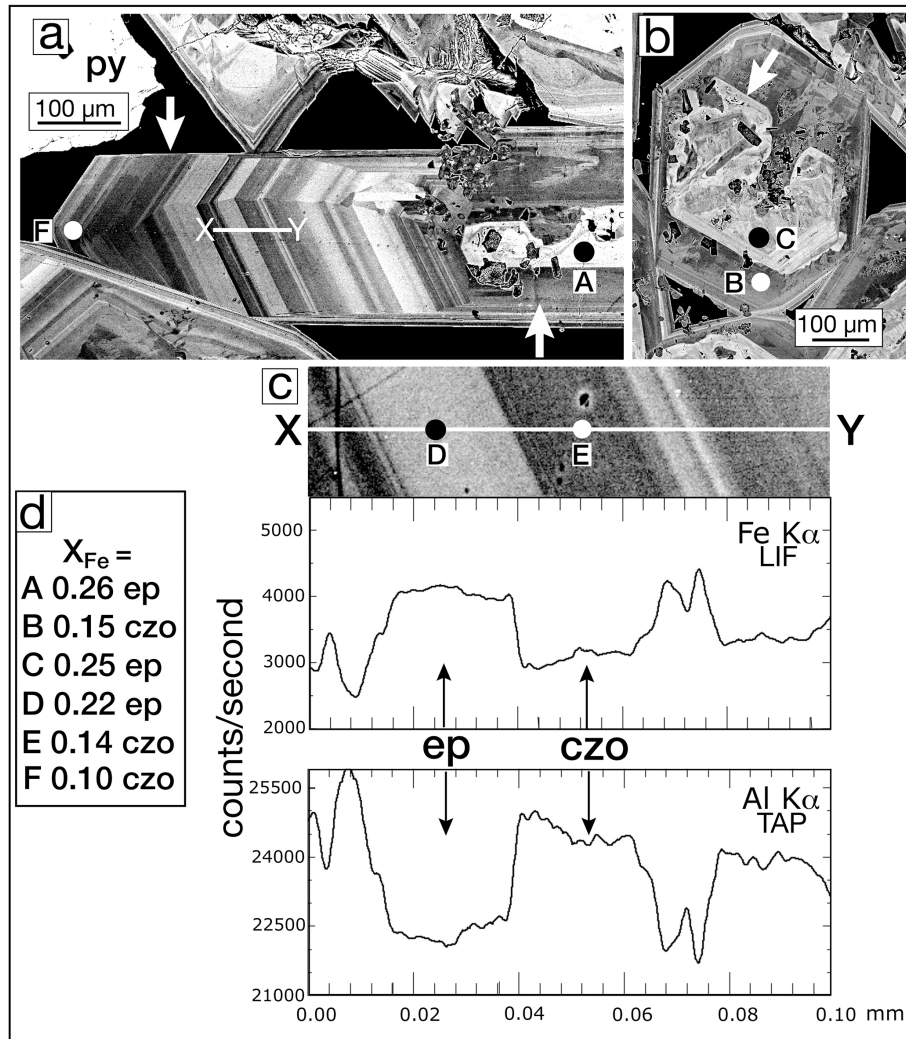
Figure 7. BSE images: **(a)** several millimeter-long, complexly zoned epidote crystals from sample SV3-2353. The left arrow indicates oscillatory growth in the *b*-crystallographic direction of the euhedral elongate crystal. The core of the crystal (right arrow) has an irregularly shaped iron-rich core. The line X–Y is the traverse shown in Fig. 7c. **(b)** A basal section of a complexly zoned epidote crystal showing an iron-rich core (arrow) that has been partially resorbed. The dark areas in the core are biotite crystals. **(c)** Enlarged detail of the EPMA traverse shown in Fig. 7a. The EPMA line traverses for the elements Fe and Al are shown below registered in position. The Fe-rich bands are epidote (ep), and Al-rich bands are clinozoisite (czo). The conditions of the EPMA line traverse were 15 keV and 30 nA, with a pixel size of ~ 0.1 µm. The excitation of the sample with the electron beam is a tear-drop-shaped volume so that as the beam traverses from one section to another, the boundaries are sloped. **(d)** Values of X_{Fe} [$(Fe^{3+}) / (Fe^{3+} + Al)$] apfu for the EPMA analytical spots A–F for epidote (ep) and clinozoisite (czo) shown in Fig. 7a, b, and c; analyses are given in Table 3.

wells than in the San Vito wells, especially in samples MF1-1597 and MF2-1824.

7.1.1 Petrography

We observed two general textures of the allanite group; (1) radiating sprays of crystals, usually at the centers of epidote group masses, and (2) groups of crystals, many euhedral, in the center of epidote group masses. These textures are authigenic, precipitated from geothermal fluids, as opposed to uncommon igneous allanite fragments we identified in the igneous products. The starburst pattern (Fig. 9a, b) was also seen without any accompanying epidote. An uncommon occurrence, only observed in sample MF1-1597, was allanite groups with cores of aluminocerite-(Ce) ($Al_2O_3 = 2.0$ wt % to 2.3 wt %) (Fig. 9c, f). Oscillatory zoned crystals (Fig. 9d) and other textures (Fig. 9e) indicate precipitation of allanite in pulses. Anenburg et al. (2015, Fig. 6a) illustrate similar oscillatory zoned allanite. Ferriallanite was only observed in one sample (MF1-1597) and forms euhedral crystals in the centers of larger epidote masses (Fig. 9f). Minor zoning of
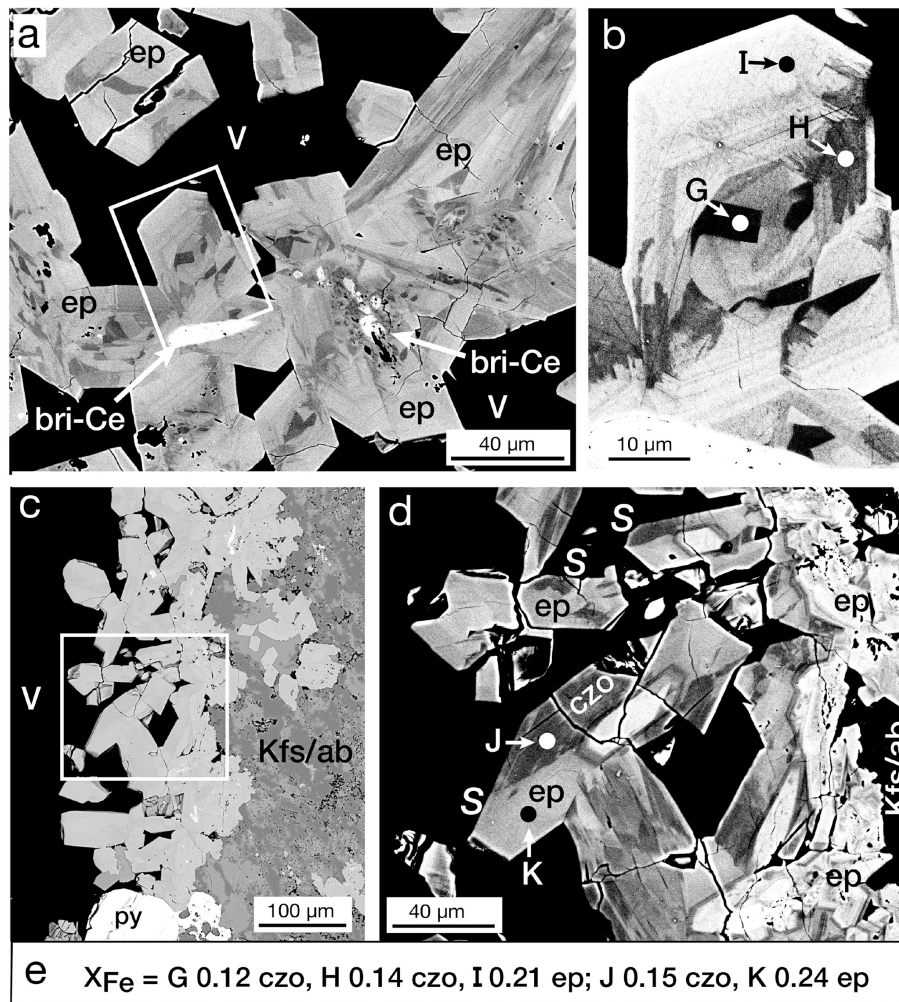
Figure 8. BSE images: **(a)** complexly zoned crystals of epidote (ep) in a vug (V) with cores of britholite-(Ce) (bri-Ce), sample MF2-1824. The rectangle is enlarged in **(b)**. **(b)** Crystal from thin section shown in **(a)** oriented vertically, illustrating complex zoning. Spots G and H are clinozoisite, and I is epidote. **(c)** Edge of a vug (V) in K-feldspar/albite (Kfs/ab) lined with complexly zoned epidote (ep) crystals, sample MF1-1597. Square enlarged in **(d)**. **(d)** Sector-zoned crystals (S) with relatively unzoned epidote cores. The sector compositions vary between epidote (ep: spot K) and clinozoisite (czo: spot J). **(e)** Values of X_{Fe} [$(Fe^{3+})/(Fe^{3+}+Al)$ apfu] for the EPMA analytical spots G–K for epidote (ep) and clinozoisite (czo) shown in Fig. 8b and d; analyses are given in Table 3.

light rare earth elements (LREEs, La–Gd) was observed in both allanite and ferriallanite.

7.1.2 Composition

The allanite and ferriallanite are enriched in LREEs and have variable compositions, mostly due to minor zoning. We did not observe any compositional relationship with temperature and/or depth. Both minerals are Ce dominant and hence are allanite-(Ce) and ferriallanite-(Ce). Minor elements analyzed in the allanite group were Ti, Mn, Mg, Sr, K, Na, Pb, Cr, Y, and Th. Manganese, Sr, Mg, and Ti are the most abundant with MnO ranging (in wt %; dl denotes detection limit) from dl–1.70, SrO ranging from dl–1.41, MgO ranging from dl–1.19, and TiO_2 ranging from dl–0.82. Potassium, Na, Y, and

Th were infrequently detected with all analyses < 0.50 wt %; Pb and Cr were not detected. The LREE abundance (in wt %) is variable: La_2O_3 varies from 3.98–8.30; Ce_2O_3 varies from 7.11–16.17; Pr_2O_3 varies from dl–1.41; Nd_2O_3 varies from 1.05–4.40. When measured, Sm_2O_3 ranges from dl–0.61, Eu_2O_3 ranges from dl–0.35, and Gd_2O_3 ranges from dl–0.37. Representative compositions of the allanite group are given in Table 4.

7.2 REE-bearing epidote group

During routine BSE observation, epidote group crystals, especially those bordering masses of allanite and ferriallanite (Fig. 9f, g), had bright rims or zones. Microprobe analysis yielded LREEs but in concentrations such that either Al or
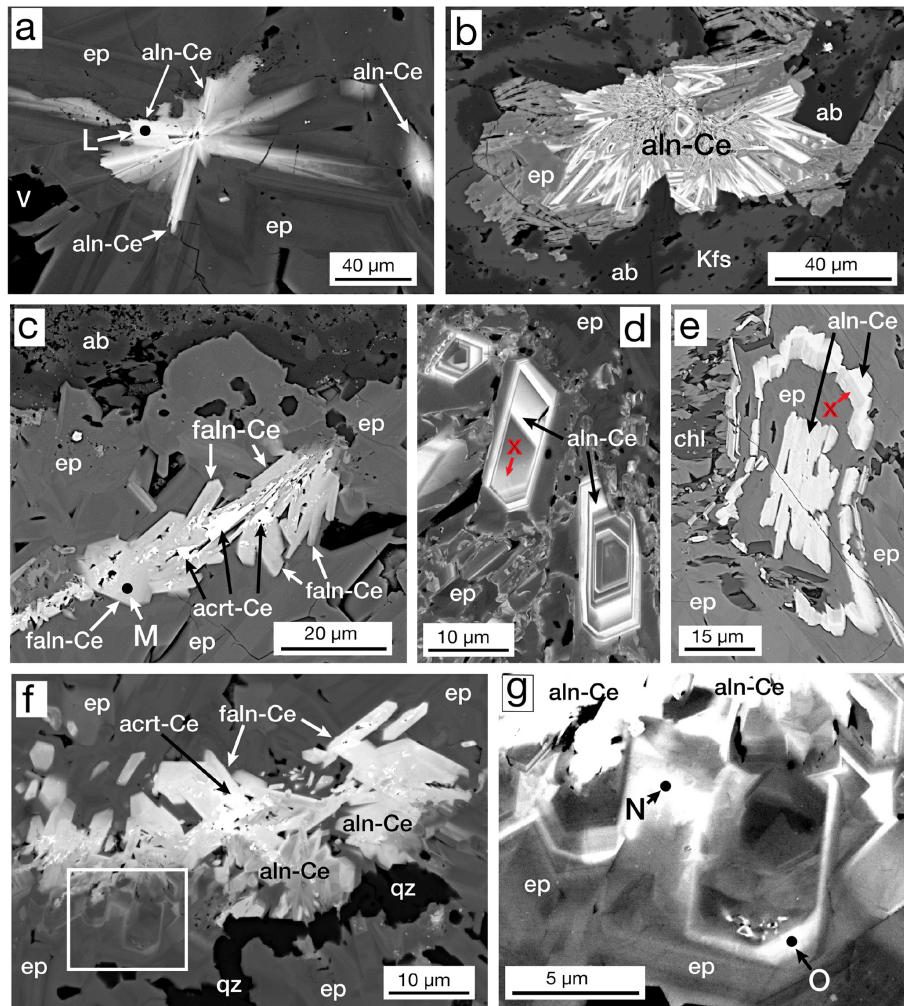
Figure 9. BSE images: **(a)** "starburst" allanite-(Ce) (aln-Ce) in the core of an epidote (ep) mass, sample MF1-1597. **(b)** Mass of radiating allanite-(Ce) (aln-Ce) with epidote (ep), albite (ab), and K-feldspar (Kfs), sample MF2-1824. **(c)** Mass of ferriallanite-(Ce) (faln-Ce) with aluminocerite-(Ce) (acrt-Ce) in their cores in an epidote (ep) mass with albite (ab), sample MF1-1597. **(d)** Zoned crystals of allanite-(Ce) (aln-Ce) with areas of REE-bearing epidote (X) in patchy REE-rich epidote (ep), sample MF2-1824. **(e)** An allanite-(Ce) core (aln-Ce) followed by epidote (ep) and then REE-bearing epidote (X) followed by allanite-(Ce) surrounded by epidote (ep) and chlorite (chl) in sample MF2-1824. **(f)** Allanite-(Ce) (aln-Ce) and ferriallanite-(Ce) (faln-Ce) in the core of a $400 \times 450 \, \mu m$ epidote (ep) mass with a late vein of quartz (qz). The rectangle is enlarged in **(g)**, sample MF1-1597. **(g)** Enlargement of area in **(f)** showing clinozoisite (czo; spot N) and epidote (ep; spot O) both enriched in LREE, just below allanite-(Ce) (aln-Ce). Data for analytical spots L–O are given in Table 4.

Fe^{3+} was dominant ($> 50 \%$ apfu) in the A2 site (Fig. 9g points N and O). In some cases, it appears that the transition from the REE-bearing epidote group to the allanite group is gradual (Fig. 9d), and in other cases, the transition seems sharp within the resolution limits of the SEM (Fig. 9e). Bonazzi and Menchetti (1995) suggest that the increasing content of Fe^{2+} in epidote distorts the structure to accommodate more REE. We observe this relationship (Table 4), but our data set is too limited to be definitive. Table 4 gives representative compositions of REE-bearing clinozoisite and epidote; all LREE compositions are Ce dominant.

8   Discussion

8.1   Geothermal epidote

Although epidote was described as a mineral species more than 180 years ago (Franz and Liebscher, 2004), the world energy "crises" of the 1970s and 1980s produced much exploration for high-enthalpy geothermal fluids for electric power production, and mineralogical studies associated with this exploration generated numerous literature descriptions of epidote from geothermal fields (e.g., Cavarretta et al., 1980, 1982; Shikazono, 1984; Bird et al., 1988). Bird and Spieler (2004) present a very comprehensive review of epi-

Table 4. Representative compositions of REE-bearing epidote supergroup minerals.

Analysis	MF2-1824xl.1	MFI-1597-1	MFI-1597-12	MFI-1597-11	MFI-1597-17	MFI-1597-19	MF2-1824-2xl.1	MFI-1597-2	MFI-1597-23-26	MFI-1597-14	MFI-1597-13	MFI-1597xl.E	SV3-2105-1
Depth (m)	1824	1597	1597	1597	1597	1597	1824	1597	1597	1597	1597	1597	2105
Comment	core						zoned with core		REE core			REE core	REE core
Figure and spot		Fig. 9a, L		Fig. 9c, M				Fig. 9g, N		Fig. 9g, O			
n	2	1	1	1	1	1	1	1	2	1	1	3	1
Mineral	aln-Ce	aln-Ce	aln-Ce	faln-Ce	faln-Ce	faln-Ce	ep	ep	ep	czo	czo	czo	czo
SiO_2 (wt %)	33.98	33.54	31.26	30.01	30.38	30.93	35.89	36.96	35.60	35.38	35.72	37.11	35.68
TiO_2	0.80	0.16	0.08	0.13	0.20	0.06	0.47	0.11	0.05	0.18	0.11	0.11	0.10
Al_2O_3	20.28	14.76	13.83	6.27	10.90	11.84	21.97	26.05	25.35	24.69	26.69	25.17	23.25
FeO^*	10.51	17.53	16.31	24.64	20.08	15.07	11.23	9.40	7.56	7.34	7.74	6.42	9.39
MgO	0.13	0.57	0.86	0.68	0.54	0.91	0.07	0.09	0.25	0.27	0.22	0.22	0.15
MnO	1.02	1.21	1.38	1.13	0.77	1.29	0.61	1.08	1.18	1.33	1.14	1.11	0.00
CaO	13.39	15.00	10.70	10.03	12.18	10.01	17.78	21.75	20.54	17.25	18.64	19.36	17.79
SrO	0.71	bdl	bdl	bdl	bdl	bdl	0.66	bdl	0.09	bdl	0.09	0.09	bdl
Na_2O	0.03	bdl	bdl	bdl	bdl	bdl	bdl	bdl	bdl	bdl	bdl	bdl	0.03
K_2O	bdl	bdl	bdl	bdl	bdl	bdl	bdl	bdl	bdl	bdl	bdl	bdl	0.02
La_2O_3	4.28	4.14	6.15	6.36	4.12	6.40	2.71	0.21	1.84	4.12	2.95	2.34	2.87
Ce_2O_3	9.04	8.86	13.05	12.76	9.81	14.03	4.62	0.56	2.77	6.31	4.59	3.20	5.05
Pr_2O_3	bdl	0.54	0.89	1.33	0.73	1.40	bdl	bdl	na	0.66	0.32	na	na
Nd_2O_3	2.04	2.36	3.69	3.81	3.22	4.13	1.10	0.24	na	1.27	1.26	0.40	1.69
Sm_2O_3	bdl	0.21	0.23	0.26	0.11	0.33	bdl	na	na	na	na	na	na
Eu_2O_3	bdl	0.16	0.12	0.31	bdl	0.17	bdl	na	na	na	na	na	na
Gd_2O_3	na	na	na	bdl	0.26	bdl	bdl	na	na	na	na	na	na
Y_2O_3	bdl	0.08	0.10	0.10	0.16	0.12	bdl	0.08	bdl	bdl	bdl	bdl	0.22
ThO_2	0.09	0.09	0.19	0.09	0.27	0.09	0.17	bdl	bdl	bdl	bdl	bdl	0.73
Total	96.25	99.21	98.93	98.05	93.73	96.78	97.28	96.53	95.23	98.81	97.93	97.05	96.97
ΣREE + Y	15.35	16.35	24.32	25.07	18.41	26.58	8.43	1.09	4.61	12.36	9.12	5.94	9.83
ΣREE + Y + Th + Sr	16.14	16.44	24.51	25.16	18.68	26.67	8.60	1.09	4.70	12.36	9.12	6.03	10.56
Formulae on the basis of (T + M + A) = 8 cations													
Si	3.064	2.993	2.973	3.001	2.983	3.076	3.032	2.946	2.937	2.970	2.957	3.021	3.031
Ti	0.054	0.011	0.006	0.010	0.015	0.004	0.030	0.007	0.003	0.011	0.008	0.007	0.006
Al	2.155	1.552	1.550	0.739	1.261	1.388	2.187	2.447	2.465	2.443	2.456	2.561	2.328
Fe^{3+}	0.686	0.904	0.638	1.058	1.070	0.772	0.423	0.615	0.515	0.300	0.337	0.205	0.268
Fe^{2+}	0.107	0.404	0.659	0.741	0.579	0.481	0.371	0.011	0.007	0.035	0.199	0.232	0.399
Mg	0.017	0.076	0.122	0.101	0.079	0.135	0.009	0.011	0.031	0.035	0.033	0.027	0.019
Mn	0.078	0.091	0.111	0.096	0.064	0.109	0.044	0.073	0.082	0.095	0.080	0.077	0.000
Ca	1.293	1.434	1.090	1.075	1.281	1.067	1.609	1.857	1.816	1.551	1.653	1.689	1.619
Sr	0.037	0.000	0.000	0.000	0.000	0.000	0.032	0.000	0.004	0.000	0.004	0.004	0.000
Na	0.004	0.000	0.000	0.000	0.000	0.000	0.000	0.000	0.000	0.000	0.000	0.000	0.005
K	0.000	0.000	0.000	0.000	0.000	0.000	0.000	0.000	0.000	0.000	0.000	0.000	0.002
La	0.142	0.136	0.216	0.235	0.149	0.235	0.084	0.006	0.056	0.128	0.090	0.070	0.090
Ce	0.298	0.289	0.454	0.467	0.353	0.511	0.143	0.016	0.084	0.194	0.139	0.095	0.157
Pr	0.000	0.018	0.031	0.048	0.026	0.051	0.000	0.000	0.000	0.020	0.010	0.000	0.000
Nd	0.066	0.075	0.125	0.136	0.113	0.147	0.033	0.007	0.000	0.038	0.037	0.012	0.051
Sm	0.000	0.006	0.008	0.009	0.004	0.011	0.000	0.000	0.000	0.000	0.000	0.000	0.000
Eu	0.000	0.005	0.003	0.011	0.000	0.006	0.000	0.000	0.000	0.000	0.000	0.000	0.000
Gd	0.000	0.000	0.000	0.000	0.008	0.000	0.000	0.000	0.000	0.000	0.000	0.000	0.000
Y	0.000	0.004	0.010	0.007	0.008	0.006	0.000	0.003	0.000	0.000	0.000	0.000	0.010
Th	0.002	0.002	0.004	0.002	0.006	0.002	0.003	0.000	0.000	0.000	0.000	0.000	0.014
ΣREE + Y	0.506	0.533	0.847	0.916	0.661	0.967	0.260	0.032	0.140	0.380	0.276	0.177	0.308
ΣREE + Y + Th + Sr	0.545	0.535	0.851	0.918	0.667	0.969	0.295	0.032	0.144	0.380	0.276	0.181	0.322

* total iron as Fe^{2+}. n, number of analyses averaged; bdl, below detection limit; na, not analyzed; Th–Lu is na. aln-Ce, allanite-(Ce); faln-Ce, ferriallanite-(Ce); ep, epidote; czo, clinozoisite; Fe^{3+}/Fe^{2+} is calculated on the basis of stoichiometry.

dote in geothermal systems and emphasize that the epidote group is common and abundant in geothermal systems at temperatures usually $> 200\,°C$, exhibits a wide range of octahedral substitution ($Al \leftrightarrow Fe^{3+}$), and displays frequent zoning. For example, Absar (1991) uses the presence of epidote to model the epidote-formation regime at $T \geq 250\,°C$ in the Ohaaki–Broadlands, New Zealand, geothermal field. Bird and Spieler (2004) and Caruso et al. (1988) emphasize the sensitive dependence of epidote composition (coupled $Al \leftrightarrow Fe^{3+}$ substitution) on temporal and spatial variations in fluid composition, redox conditions, pH, CO_2 concentrations, aqueous speciation of Fe and Al complexes, etc. Bird and Spieler (2004, p. 284) conclude their review by warning the epidote researcher that "interpretation of the chemical and physical evolution of magma-hydrothermal systems based on chemically zoned epidotes must be considered with caution".

8.2 Epidote composition and well temperature

Figure 6a and b show the co-variation in X_{Fe} with temperature for the Mofete and San Vito wells. The San Vito system has been disturbed by faulting, and this is evident by the distribution of epidote compositions, structural relations, and drill-hole stratigraphy (Chelini and Sbrana, 1987; De Vivo et al., 1989). In contrast, the Mofete system has been described as a simple, generally prograde, active, and structurally undisturbed area. Although there is scatter, we found decreasing X_{Fe} with increasing well temperature and more clinozoisite below $320\,°C$. De Vivo et al. (1989) assessed the fossil temperature variation in the boreholes by fluid inclusion microthermometry for comparison with the measured well temperature. The fluid inclusion data indicate relatively stable thermal conditions for MF1, MF2, and SV1, but the data suggest that the thermal regime in well MF5 has cooled subsequent to fluid inclusion trapping and host mineral crystallization. Overlapping mineral assemblage zones in the SV3 well indicate that minerals that hosted the measured fluid inclusions are relatively recent and that a significantly hotter regime existed in the past (De Vivo et al., 1989). Guglielminetti (1986) and De Vivo et al. (1989) describe multiple fluid reservoirs in the Mofete field characterized by differences in the salinity and total dissolved solids (TDSs), but we did not observe any effect of these differences on the chemistry of distribution of the epidote supergroup.

Liou (1973) suggests that Al increases in epidote with increasing temperature on the basis of experimental studies. Poli and Schmidt (2004) remark that generally epidote becomes more aluminous as oxygen fugacity decreases, but this relationship was equivocal. Potel et al. (2002) also describe epidote composition in New Caledonia metamorphics that varies as a function of oxygen fugacity and that rock composition is the main factor that controls both mineral assemblages and their composition. Liou et al. (1985), Caruso et al. (1988), and Arnason and Bird (1992) report decreas-

ing X_{Fe} with increasing temperature and/or depth, whereas Shearer et al. (1988) report no systematic variation with depth. In fact, many descriptions of geothermal epidote report no relationship between X_{Fe} and temperature and/or depth and describe complex epidote histories, such as multiple generations, and disequilibrium mineral assemblages (Bird and Spieler, 2004, and references therein). In particular, Bird and Spieler (2004) illustrate the complexity of the influence of these variables by pointing out that the Al content of epidote will both increase and decrease with increasing temperature as a function of CO_2 fugacity (e.g., Arnason et al., 1993).

Iron in the Mofete and San Vito geothermal fluids was a mixture of Fe^{2+} and Fe^{3+} as there was common simultaneous precipitation of various divalent iron sulfides with epidote group minerals. We also identified iron oxides in all the samples. Hematite, intergrown with epidote (Fig. 4d), was observed in some samples, and this suggests mineralization from more oxidizing fluids as also suggested by McKibben et al. (1988) for the Salton Sea geothermal system. The sulfur fugacity also varied although from the restricted occurrence of anhydrite, most sulfur was relatively reduced. However, the fact that a general decrease in X_{Fe} with increasing temperature is observed at all, especially in the MF1 well, suggests that the most important factors that determined X_{Fe} distribution have remained relatively constant during the formation of the measured epidote group.

8.3 Zoning

Zoning in rock-forming minerals was described in the 19th century from some of the first petrographic studies of rocks using polarized light microscopy (e.g., Sorby, 1858). Different types of zoning have been subsequently recognized, and various theories have been put forward to explain the various types of zoning. Some reported epidote zoning seems related to the host rock composition where, for example, more iron-rich host rocks produce more iron-rich epidotes (Shikazono, 1984), whereas in other epidote studies (Santaguida, 1999) where host rock composition widely varies, no relationship was observed. De Vivo et al. (1989) and Chelini and Sbrana (1987) indicate no significant differences in host rock composition with regard to iron content in the Campi Flegrei lithologies from which the studied samples were selected.

Relatively simple zoning, where epidote crystals have either Al-rich or Fe-rich rims, has been explained by Arnason and Bird (1992) as the reaction path for plagioclase and calcite dissolution, respectively. Arnason and Bird (1992) also emphasize the sensitivity of epidote composition to such factors as pH and Fe^{3+} and Al speciation. The complex and widely varied epidote zoning observed in the Campi Flegrei samples suggests complicated and relatively rapid fluctuation in intensive parameters to produce a great variability in zoning. Furthermore, epidote crystal chemical sites, such as M1,

M2, and M3, seem to be especially sensitive to these condition changes.

Oscillatory zoning can arise from various oscillations in the growth medium (Loomis, 1983) or by autonomous, time-independent oscillations that are self-organized such as those in reaction–diffusion systems, like the Belousov–Zhabotinsky reaction type (Ortoleva, 1994). Figure 7a shows a typical epidote crystal with well-developed oscillatory zoning. A detailed, high-resolution SEM–BSE examination of the oscillatory zones in the Campi Flegrei epidotes did not show any sawtooth periodic decay, nor did it show any other pattern typical of those described in self-organized zoning. The oscillatory zoning was separated by sharp interfaces, and in any single band, the composition was usually uniform within the limits of the available instruments (Fig. 7a, c). The alternation of Fe-rich and Fe-poor bands suggests oscillations in the fluid media such as rapid changes in pH, $f\mathrm{CO_2}$, $f\mathrm{O_2}$, or composition. The sharpness of the individual zones, at least on the scale of the SEM resolution, suggests that the fluid diffusion rates for the local conditions surrounding the growing crystals were rapid, but the solid diffusion rates were essentially zero with respect to this environment. No resorbed edges among the oscillatory bands were seen in the studied samples, suggesting a relatively rapid prograde environment.

Oscillatory zoning in epidote is common (e.g., Janeczek and Sachanbinski, 1992; Choo, 2002; Inoue and Utada, 2017; Bird and Spieler, 2004, and references therein). Choo (2002) describes oscillatory zoning in the Bobae sericite deposits, and microprobe experiments across oscillatory bands yield amplitudes which range from 2 to 13 X_{Fe}. This is the general range measured in the oscillatory zoned epidote group in the present study (4–10 X_{Fe}).

Sector zoning is zoning localized at particular crystallographic orientations with differences in composition between sectors. Dowty (1976) discusses this zoning type with respect to epidote formation and indicates that the M1 and M2 sites prefer Al very strongly over $\mathrm{Fe^{3+}}$, whereas the M3 site prefers $\mathrm{Fe^{3+}}$, although Fehr and Heuss-Aßbichler (1999) suggest that the M2 is occupied by Al exclusively. Sector zoning in epidote can be quite complex: Yoshizawa (1984) describes an example in a low-grade schist where the epidote is zoned in 10 different crystallographic sectors. Thus, epidote growth in a fluid with both Fe and Al species available may produce zones controlled by crystallographic compositional differences. However, other factors need to be favorable to develop sector zoning; probably a relatively stagnant fluid is needed for the site-selective compositional differences to be operative. For example, Fig. 8d shows sector zoning in some sample areas although interfering crystal growth areas have complicated the pattern.

Complex zoning, the most common type observed in the Campi Flegrei epidotes, is a mixture of oscillatory banding, sector zoning, and patchy growth. Figure 8a and b show typical complexly zoned epidotes in vugs, and Fig. 4f shows this

zoning type in a vein. Zoning of any type was more common in the deeper, hotter parts of the Campi Flegrei geothermal field, but this also may, in part, be influenced by the fact that epidote was also more abundant.

Thus, there are two sources of compositional variability identified in this study: one related to oscillatory zoning in response to intensive parameter and or fluid composition change and the other related to crystallographic features such as sector zoning.

8.4   REE-bearing epidote supergroup and REEs in geothermal fluids

Allanite-(Ce) was commonly observed in the Mofete samples but was less abundant in the San Vito samples. Ferriallanite was only identified in one Mofete sample, MF1-1597. The distribution and abundance of the REE-bearing epidote group (epidote and clinozoisite) follow those of the allanite group.

During SEM–EDS petrographic study we identified the following geothermal authigenic REE-bearing minerals: zircon, zirconolite, synchysite-(Ce), bastnäsite-(Ce), monazite-(Ce), cerite-(Ce), aluminocerite-(Ce), britholite-(Ce), and probable hellandite-(Y); all except zircon and zirconolite were LREE enriched. We also noted the presence of authigenic fluorite and fluorapatite in the samples, attesting to F as a component of the geothermal fluids. Mormone et al. (2011) report allanite in MF1 and a REE phosphate in MF5, and Piochi et al. (2021) identified an La- and Ce-bearing epidote in SV1 at 1713 m depth; no analyses of any of these REE phases are given.

Unfortunately, we know of no analyses of REEs in the geothermal fluids sampled during the drilling of the Mofete and San Vito wells (De Vivo et al., 1989) or any other nearby geothermal wells (Somma et al., 2021) or thermal springs and fumaroles (Valentino et al., 1999). However, REEs have been analyzed in high-temperature fluids from the Larderello–Travale and Monte Amiata geothermal fields, Tuscany, Italy (Möller, 2002), and from the Reykjanes geothermal system, Iceland (Fowler and Zierenberg, 2015). In these two studies, the REEs were LREE enriched with some variation in the degree of enrichment. Williams-Jones (2015) indicates that LREEs form more stable complexes in chloride and fluoride solutions than in heavy rare earth elements (HREEs, Tb–Lu). This is compatible with the San Vito and Mofete geothermal saline fluids (De Vivo et al., 1989) and the common presence of fluorite and fluorapatite.

9   Conclusions

We conclude the following. (1) Authigenic epidote group minerals, epidote and clinozoisite, are common to abundant in the calcium–aluminum silicate and thermometamorphic zones of the Mofete and San Vito geothermal fields,

Campi Flegrei, Italy. (2) Their compositions encompass nearly the complete range of coupled $Al \leftrightarrow Fe^{3+}$ substitution from X_{Fe} 0.06 to 0.33 (Fe^{3+} = 0.185–0.967 apfu), and in the Mofete wells, X_{Fe} tended to decrease with increasing temperature and depth. (3) The measured well temperatures ranged from 275–350 °C and 300–390 °C in the Mofete and San Vito wells, respectively, although the fluid inclusion study by De Vivo et al. (1989) indicates some differences in past temperatures. (4) Oscillatory, sector, and complex zoning are ubiquitous and indicate rapid changes in one or more intensive parameters. (5) Two members of the allanite group, allanite-(Ce) and ferriallanite-(Ce), were identified; their texture indicates that they are authigenic and that the geothermal fluids were enriched in, at least, LREEs. REE-bearing epidote and clinozoisite were observed, usually in proximity to the allanite group.

References

Absar, A.: Hydrothermal epidote – An indicator of temperature and fluid composition, J. Geol. Soc. India, 38, 625–628, 1991.

Aggarwal, J.: Fractionation of rare earth elements into hydrothermal epidotes: An examination of crystallographic controls, J. Conf. Abstracts, 4, 722, 1991.

Ahmed, A. D., Fisher, L., Pearce, M., Escolme, A., Cooke, D. R., Howard, D., and Belousov, I.: A microscale analysis of hydrothermal epidote: Implications for the use of laser ablation-inductively coupled plasma-mass spectrometry mineral chemistry in complex alteration environments, Econ. Geol., 115, 793–811, https://doi.org/10.5382/econgeo.4705, 2020.

Altaner, S. P., Lander, R. H., Klimentidis, R. E., and Ylagan, R. F.: Hydrothermal alteration in two active geothermal wells from the Phlegrean volcanic fields, Italy, 28th Annual Clay Minerals Society Meeting, Houston, TX, , Lunar and Planetary Institute, Houston, TX, 5–10 October, 28, 4, 1991.

Anenburg, M., Katzir, Y., Rhede, D., Jöns, N., and Bach, W.: Rare earth element evolution and migration in plagiogranites: a record preserved in epidote and allanite of the Troodos ophiolite, Contrib. Mineral. Petr., 169, 25, https://doi.org/10.1007/s00410-015-1114-y, 2015.

Armbruster, T., Bonazzi, P., Akasaka, M., Bermanec, V., Chopin, C., Gieré, R., Heuss-Assbichler, S., Liebscher, A., Menchetti, S., Pan, Y., and Pasero, M.: Recommended nomenclature of epidote-group minerals, Eur. J. Mineral., 18, 551–567, https://doi.org/10.1127/0935-1221/2006/0018-0551, 2006.

Armstrong, J. T.: CITZAF: A package of correction programs for the quantitative electron microbeam X-ray analysis of thick polished materials, thin ?lms, and particles, Microb. Anal., 4, 177–200, 1995.

Arnason, J. G. and Bird, D. K.: Formation of zoned epidote in hydrothermal systems, Proceedings of the 7th International Symposium on Water-Rock Interaction, Park City, Utah, USA, 13–18 July 1992, 1473–1476, A. A. Balkema, Rotterdam, Netherlands, ISBN 9789054100775, 1992.

Arnason, J. G., Bird, D. K., and Liou, J. G.: Variables controlling epidote composition in hydrothermal and low-pressure regional metamorphic rocks, Proceedings of a Symposium held in Neukirchen am Großvenediger, Salzburg, Austria, September 1990, Abh. Geol. B-A., 49, 17–25, 1993.

Bagnato, E., Tamburello, G., Granieri, D., Caliro, S., D'Agostino, F., Avino, R., Capecchiacci, F., Carandente, A., D'Alessandro, A., Minopoli, C., and Santi, A.: First simultaneous mercury and major volatiles characterization of atmospheric hydrothermal emissions at the Pisciarelli's fumarolic system (Campi Flegrei, Italy), J. Volcanol. Geoth. Res., 406, 107074, https://doi.org/10.1016/j.jvolgeores.2020.107074 2020.

Belkin, H. E. and De Vivo, B.: Compositional variation of epidote in the Campi Flegrei geothermal field, Naples, Italy, 13th Annual V.M. Goldschmidt Conference, Copenhagen, Denmark, 5–11 June 2004, 68, A268, https://doi.org/10.1016/j.gca.2004.05.001, 2004.

Belkin, H. E., Caprarelli, G., and De Vivo, B.: The Campi Flegrei (Italy) geothermal system: Epidote chemistry and radiogenic isotopes, Eos Trans. Amer. Geophys. Union, 71, 1686, https://doi.org/10.1029/EO071i043p01219, 1990.

Belkin, H. E., Rolandi, G., Jackson, J. C., Cannatelli, C., Doherty, A. L., Petrosino, P., and De Vivo, B.: Mineralogy and

geochemistry of the older (> 40 ka) ignimbrites on the Campanian Plain, southern Italy, J. Volcanol. Geoth. Res., 323, 1–18, https://doi.org/10.1016/j.jvolgeores.2016.05.002, 2016.

Bird, D. K. and Spieler, A. R.: Epidote in Geothermal Systems, in: Reviews in Mineralogy and Geochemistry, Vol. 56, Epidotes, edited by: Liebscher, A. and Franz, G., Mineralogical Society of America and Geochemical Society, Washington, DC, USA, 235–300, https://doi.org/10.2138/gsrmg.56.1.235, 2004.

Bird, D. K., Cho, M., Janik, C. J., Liou, J. G., and Caruso, L. J.: Compositional, Order/Disorder, and Stable Isotope Characteristics of Al-Fe Epidote, State 2–14 Drill Hole, Salton Sea Geothermal System, J. Geophys. Res.-Sol. Ea., 93, 13135–13144, https://doi.org/10.1029/JB093iB11p13135, 1988.

Bodnar, R. J., Cannatelli, C., De Vivo, B., Lima, A., Belkin, H. E., and Milia, A.: Quantitative model for magma degassing and ground deformation (bradyseism) at Campi Flegrei, Italy: Implications for future eruptions, Geology, 35, 791–794, https://doi.org/10.1130/G23653A.1, 2007.

Bonazzi, P. and Menchetti, S.: Monoclinic members of the epidote group: effects of the Al Fe^{3+} Fe^{2+} substitution and of the entry of REE^{3+}, Mineral. Petrol., 53, 133–153, https://doi.org/10.1007/BF01171952, 1995.

Brunsmann, A., Franz, G., and Heinrich, W.: Experimental investigation of zoisite-clinozoisite phase equilibria in the system CaO-Fe$_2$O$_3$-Al$_2$O$_3$-SiO$_2$-H$_2$O, Contrib. Mineral. Petrol., 143, 115–130, https://doi.org/10.1007/s00410-001-0335-4, 2002.

Caprarelli, G., Tsutsumi, M., and Turi, B.: Chemical and isotopic signatures of the basement rocks from the Campi Flegrei geothermal field (Naples, southern Italy); inferences about the origin and evolution of its hydrothermal fluids, J. Volcanol. Geoth. Res., 76, 63–82, https://doi.org/10.1016/S0377-0273(96)00072-8,1997.

Carlino, S., Somma, R., Troise, C., and De Natale, G.: The geothermal exploration of Campanian volcanoes: Historical review and future development, Renew. Sust. Energ. Rev., 16, 1004–1030, https://doi.org/10.1016/j.rser.2011.09.023, 2012.

Caruso, L. J., Bird, D. K., Cho, M., and Liou, J. G.: Epidote-Bearing Veins in the State 2–14 Drill Hole: Implications for Hydrothermal Fluid Composition, J. Geophys. Res-Sol. Ea., 93, 13123–13133, https://doi.org/10.1029/JB093iB11p13123, 1988.

Cavarretta, G., Gianelli, G., and Puxeddu, M.: Hydrothermal metamorphism in the Larderello geothermal field, Geothermics, 9, 297–314, https://doi.org/10.1016/0375-6505(80)90008-5, 1980.

Cavarretta, G., Gianelli, G., and Puxeddu, M.: Formation of authigenic minerals and their use as indicators of the physicochemical parameters of the fluid in the Larderello-Travale geothermal field, Econ. Geol., 77, 1071–1084, https://doi.org/10.2113/gsecongeo.77.5.1071, 1982.

Chelini, W. and Sbrana, A.: Subsurface geology, in: Phlegrean Fields, edited by: Rosi, M. and Sbrana, A., Consiglio Nazionale delle Ricerche, Quaderni De La Ricerca Scientifica, Roma, Italy, 94–103, ISSN 0556-9664, 1987.

Chen, A. P., Yang, J. J., Zhong, D. L., Shi, Y. H., and Liu, J. B.: Epidote spherulites and radial euhedral epidote aggregates in a greenschist facies metavolcanic breccia hosting an UHP eclogite in Dabieshan (China): Implication for dynamic metamorphism, Am. Mineral., 104, 1197–1212, https://doi.org/10.2138/am-2019-6980, 2019.

Chiodini, G., Caliro, S., Avino, R., Bagnato, E., Capecchiacci, F., Carandente, A., Cardellini, C., Minopoli, C., Tamburello, G.,

Tripaldi, S., and Aiuppa, A.: The Hydrothermal System of the Campi Flegrei Caldera, Italy, in: Campi Flegrei, edited by: Orsi, G., D'Antonio, M., and Civetta, L., Springer, Berlin, Heidelberg, 239–255, https://doi.org/10.1007/978-3-642-37060-1_9, 2022.

Choo, C. O.: Complex compositional zoning in epidote from rhyodacitic tuff, Bobae sericite deposit, southeastern Korea, Neues Jb. Miner. Abh., 177, 181–197, https://doi.org/10.1127/0077-7757/2002/0177-0181, 2002.

Dawes, R. L.: Evidence from rare earth zoning in magmatic epidote for assimilation of peraluminous granulite by dacitic magmas at 30 km depth, Eos, Trans. Amer. Geophys. Union, 71, 1144, https://doi.org/10.1029/EO071i043p01219, 1990.

Deer, W. A., Howie, R. A., and Zussman, J. (Eds.): Disilicates and Ring Silicates, Vol. 1B, 2nd Edn., Longman Scientific and Technical, Essex, United Kingdom, ISBN 0582465214, 1986.

De Vivo, B., Belkin, H. E., Barbieri, M., Chelini, W., Lattanzi, P., Lima, A., and Tolomeo, L.: The Campi Flegrei (Italy) geothermal system: a fluid inclusion study of the Mofete and San Vito fields, J. Volcanol. Geoth. Res., 36, 303–326, https://doi.org/10.1016/0377-0273(89)90076-0, 1989.

De Vivo, B. and Lima, A.: A hydrothermal model for ground movements (bradyseism) at Campi Flegrei, Italy, in: Volcanism in the Campania Plain – Vesuvius, Campi Flegrei and Ignimbrites, edited by: De Vivo, B., Elsevier, Amsterdam, the Netherlands, 289–317, https://doi.org/10.1016/S1871-644X(06)80028-8, 2006.

De Vivo, B., Rolandi, G., Gans, P. B., Calvert, A., Bohrson, W. A., Spera, F. J., and Belkin, H. E.: New constraints on the pyroclastic eruptive history of the Campanian volcanic Plain, (Italy), Miner. Petrol., 73, 47–65, https://doi.org/10.1007/s007100170010, 2001.

De Vivo, B., Belkin, H. E., and Rolandi, G. (Eds.): Vesuvius, Campi Flegrei, and Campanian Volcanism, Elsevier, Amsterdam, the Netherlands, ISBN 9780128164549, 2020.

Dowty, E.: Crystal structure and crystal growth: II. Sector zoning in minerals, Am. Mineral., 61, 460–469, 1976.

Exley, R. A.: Microprobe studies of REE-rich accessory minerals: Implications for Skye granite petrogenesis and REE mobility in hydrothermal systems, Earth Planet. Sc. Lett., 48, 97–110, https://doi.org/10.1016/0012-821X(80)90173-9, 1980.

Fehr, K.-T. and Heuss-Aßbichler, S.: Kinetics of ordering processes in epidote solid solution along the join clinozoisite-epidote, J. Conf. Abstracts, 4, 720, 1999.

Fowler, A. P. and Zierenberg, R. A.: Rare earth element concentrations in geothermal fluids and epidote from the Reykjanes geothermal system, Iceland, in: Proceedings World Geothermal Congress 2015, International Geothermal Association, Den Haag, the Netherlands, Melbourne, Australia, 19–25 April 2015, 1–11, ISBN 1877040029, 2015.

Franz, G. and Liebscher, A.: Physical and chemical properties of the epidote minerals – An introduction, in: Reviews in Mineralogy and Geochemistry, Vol. 56, Epidotes, edited by: Liebscher, A. and Franz, G., Mineralogical Society of America and Geochemical Society, Washington, DC, USA, 1–81, https://doi.org/10.2138/gsrmg.56.1.1, 2004.

Giacomelli, L. and Scandone, R.: History of the exploitation of thermo-mineral resources in Campi Flegrei and Ischia, Italy, J. Volcanol. Geoth. Res., 209, 19–32, https://doi.org/10.1016/j.jvolgeores.2011.10.004, 2012.

Gieré, R. and Sorensen, S. S.: Allanite and other REE-rich epidote-group minerals, in: Reviews in Mineralogy and Geochemistry, Vol. 56, Epidotes, edited by: Liebscher, A. and Franz, G., Mineralogical Society of America and Geochemical Society, Washington, DC, USA, 431–493, https://doi.org/10.2138/gsrmg.56.1.431, 2004.

Guglielminetti, M.: Mofete geothermal field, Geothermics, 15, 781–790, https://doi.org/10.1016/0375-6505(86)90091-X, 1986.

Guidi, A., and Antonelli, G.: Modeling in the Mofete field, in: European Geothermal Update, edited by: Louwrier, K., Staroste, E., Garnish, J. D., and Karkoulias, V., Kluwer Academic Publishers, Dordrecht, the Netherlands, 119–128, ISBN 0792301986, 1989.

Holdaway, M. J.: Thermal stability of Al-Fe epidote as a function of fO$_2$ and Fe content, Contrib. Mineral. Petr., 37, 307–340, https://doi.org/10.1007/BF00371011, 1972.

Huebner, J. S. and Woodruff, M. E.: Chemical compositions and critical evaluation of microprobe standards available from the Reston microprobe facility, U.S. Geological Survey Open File Report 85-718, 45 pp., https://doi.org/10.3133/ofr85718, 1985.

Inoue, A. and Utada, M.: Pinkish colored epidotes found in a geothermal exploration well NB–1, Noboribetsu, Hokkaido, J. Miner. Petrol. Sci., 112, 147–158, https://doi.org/10.2465/jmps.161229, 2017.

Janeczek, J. and Sachanbinsk, M.: Babingtonite, Y-Al-rich titanite, and zoned epidote from the Strzegom pegmatites, Poland, Eur. J. Mineral., 307–320, Eur. J. Mineral., https://doi.org/10.1127/ejm/4/2/0307, 1992.

Lima, A., De Vivo, B., Spera, F. J., Bodnar, R. J., Milia, A., Nunziata, C., Belkin, H. E., and Cannatelli, C.: Thermodynamic model for uplift and deflation episodes (bradyseism) associated with magmatic-hydrothermal activity at Campi Flegrei, Italy, Earth Sci. Rev., 97, 44–58, 2009.

Lima, A., Bodnar, R. J., De Vivo, B., Spera, F. J., and Belkin, H. E.: Interpretation of Recent Unrest Events (Bradyseism) at Campi Flegrei, Napoli (Italy): Comparison of Models Based on Cyclical Hydrothermal Events versus Shallow Magmatic Intrusive Events, Geofluids, 2021, 1–16, https://doi.org/10.1155/2021/2000255, 2021.

Liou, J. G.: Synthesis and stability relations of epidote, Ca$_2$Al$_2$FeSi$_3$O$_{12}$(OH), J. Petrol., 14, 381–413, https://doi.org/10.1093/petrology/14.3.381, 1973.

Liou, J. G., Seki, Y., Guillemette, R. N., and Sakai, H.: Compositions and parageneses of secondary minerals in the Onikobe geothermal system, Japan, Chem. Geol., 49, 1–20, https://doi.org/10.1016/0009-2541(85)90143-3, 1985.

Loomis, T. P.: Compositional zoning of crystals: A record of growth and reaction history, in: Kinetic and equilibrium in mineral reactions, edited by: Saxena, S. K., Springer-Verlag, New York, NY, USA, 1–60, https://doi.org/10.1007/978-1-4612-5587-1_1, 1983.

McKibben, M. A., Andes Jr., J. P., and Williams, A. E.: Active ore formation at a brine interface in metamorphosed deltaic lacustrine sediments; the Salton Sea geothermal system, California, Econ. Geol., 83, 511–523, https://doi.org/10.2113/gsecongeo.83.3.511, 1988.

Mills, S. J., Hatert, F., Nickel, E. H., and Ferraris, G.: The standardisation of mineral group hierarchies: application to recent nomenclature proposals, Eur. J. Mineral., 21, 1073–1080, https://doi.org/10.1127/0935-1221/2009/0021-1994, 2009.

Möller, P.: Rare earth elements and yttrium in geothermal fluids, Water Trans., 40, 97–125, 2002.

Mormone, A., Tramelli, A., Di Vito, M. A., Piochi, M., Troise, C., and De Natale, G.: Secondary hydrothermal minerals in buried rocks at the Campi Flegrei caldera, Italy: a possible tool to understand the rock-physics and to assess the state of the volcanic system, Period. Mineral., 80, 385–406, https://doi.org/10.2451/2011PM0027, 2011.

Orsi, G., D'Antonio, M., and Civetta, L., (Eds.): Campi Flegrei – A Restless Caldera in a Densely Populated Area, Springer, Berlin, Germany, ISBN 3642370594, 2022.

Ortoleva, P. J.: Geochemical Self-Organization, Oxford University Press, New York, NY, USA, ISBN 0195044762, 1994.

Patrier, P., Beaufort, D., Touchard, G., and Fouillac, A.-M.: Crystal size of epidotes: A potentially exploitable geothermometer in geothermal fields?, Geology, 18, 1126–1129, https://doi.org/10.1130/0091-7613(1990)018<1126:CSOEAP>2.3.CO;2, 1990.

Piochi, M., Kilburn, C. R. J., Di Vito, M. A., Mormone, A., Tramelli, A., Troise, C., and De Natale, G.: The volcanic and geothermally active Campi Flegrei caldera: an integrated multidisciplinary image of its buried structure, Int. J. Earth Sci., 103, 401–421, https://doi.org/10.1007/s00531-013-0972-7, 2014.

Piochi, M., Cantucci, B., Montegrossi, G., and Currenti, G.: Hydrothermal Alteration at the San Vito Area of the Campi Flegrei Geothermal System in Italy, Mineral Review and Geochemical Modeling, Minerals, 11, 810, https://doi.org/10.3390/min11080810, 2021.

Poli, S. and Schmidt, M. W.: Experimental subsolidus studies on epidote minerals, in: Reviews in Mineralogy and Geochemistry, Vol. 56, Epidotes, edited by: Liebscher, A. and Franz, G., Mineralogical Society of America and Geochemical Society, Washington, DC, USA, 171–195, https://doi.org/10.2138/gsrmg.56.1.171, 2004.

Potel, S., Schmidt, S. T., and de Capitani, C.: Composition of pumpellyite, epidote and chlorite from New Caledonia. How important are metamorphic grade and whole-rock composition?, Schweiz. Miner. Petrog., 82, 229–252, https://doi.org/10.5169/seals-62363, 2002.

Rolandi, G., Bellucci, F., Heizler, M. T., Belkin, H. E., and De Vivo, B.: Tectonic controls on the genesis of ignimbrites from the Campanian Volcanic Zone, southern, Italy, Miner. Petrol., 79, 3–31, https://doi.org/10.1007/s00710-003-0014-4, 2003.

Rolfo, F., Compagnoni, R., Xu, S., and Jiang, L.: First report of felsic whiteschist in the ultrahigh-pressure metamorphic belt of Dabie Shan, China, Eur. J. Mineral., 12, 883–898, https://doi.org/10.1127/0935-1221/2000/0012-0883, 2000.

Rosi, M. and Sbrana, A. (Eds.): Phlegrean Fields, Consiglio Nazionale delle Ricerche, Quaderni de La Ricerca Scientifica 114, Consiglio Nazionale delle Ricerche, Roma, Italy, 1987.

Santaguida, F.: The paragenetic relationships of epidote-quartz hydrothermal alteration within the Noranda volcanic complex, Quebec, Ph.D. dissertation, Department of Earth Sciences, Carleton University, Ottawa, ON, Canada, 302 pp., https://doi.org/10.22215/etd/1999-04190, 1999.

Scherrer, N. C., Engi, M., Gnos, E., Jakob, V., and Leichti, A.: Monazite analysis; from sample preparation to microprobe age dating and REE quantification, Schweiz. Miner. Petrog., 80, 93–105, 2000.

Shearer, C. K., Papike, J. J., Simon, S. B., Davis, B. L, and Laul, J. C.: Mineral reactions in altered sediments from the California State 2–14 well: Variations in the modal mineralogy, mineral chemistry and bulk composition of the Salton Sea Scientific Drilling Project core, J. Geophys. Res.-Sol. Ea., 93, 13104–13122, https://doi.org/10.1029/JB093iB11p13104, 1988.

Shikazono, N.: Compositional variations in epidote from geothermal areas, Geochem. J., 18, 181–187, https://doi.org/10.2343/geochemj.18.181, 1984.

Smulikowski, W. and Kozłowski, A.: Distribution of cerium, lanthanum and yttrium in allanites and associated epidotes of metavolcanic rocks of Hornsund area, Vestspitzbergen, Neues Jb. Miner. Abh., 166, 295–324, 1994.

Somma, R., Blessent, D., Raymond, J., Constance, M., Cotton, L., Natale, G. D., Fedele, A., Jurado, M. J., Marcia, K., Miranda, M., and Troise, C.: Review of recent drilling projects in unconventional geothermal resources at Campi Flegrei Caldera, Cornubian Batholith, and Williston Sedimentary Basin, Energies, 14, 3306, https://doi.org/10.3390/en14113306, 2021.

Sorby, H. C.: On the microscopic structure of crystals, indicating the origin of minerals and rocks, Q. J. Geol. Soc. Lond., 14, 453–500, https://doi.org/10.1144/GSL.JGS.1858.014.01-02.44, 1858.

Valentino, G. M., Cortecci, G., Franco, E., and Stanzione, D.: Chemical and isotopic compositions of minerals and waters from the Campi Flegrei volcanic system, Naples, Italy, J. Volcanol. Geoth. Res., 91, 329–344, https://doi.org/10.1016/S0377-0273(99)00042-6, 1999.

Williams-Jones, A. E.: The hydrothermal mobility of the rare earth elements, in: Symposium on Strategic and Critical Materials Proceedings, British Columbia Geological Survey Paper 2015-3, Victoria, BC, Canada, 13–14 November 2015, 119–123, 2015.

Yavuz, F. and Yildirim, D. K.: A Windows program for calculation and classification of epidote-supergroup minerals, Period. Mineral., 87, 269–285, 2018.

Yoshizawa, H.: Notes on petrography and rock-forming mineralogy (16) Sector-zoned epidote from Sanbagawa schist in central Shikoku, Japan, J. Miner. Petrol. Sci., 79, 101–110, https://doi.org/10.2465/ganko1941.79.101, 1984.

Zamora, M., Sartoris, G., and Chelini, W.: Laboratory measurements of ultrasonic wave velocities in rocks from the Campi Flegrei volcanic system and their relation to other field data, J. Geophys. Res., 99, 13553–13561, https://doi.org/10.1029/94JB00121, 1994.

Zen, E.-A. and Hammarstrom, J. M.: Magmatic epidote and its petrologic significance, Geology, 12, 515–518, https://doi.org/10.1130/0091-7613(1984)12<515:MEAIPS>2.0.CO;2, 1984.